國立臺灣大學電機資訊學院電子工程研究所

碩士論文

Graduate Institute of Electronics Engineering

College of Electrical Engineering and Computer Science

National Taiwan University

Master Thesis

同心圓金氧半穿隧二極體耦合效應在光傳感中的應用

Applications of Concentric MIS(p) Tunnel Diode Coupling Effect on Photo Sensing

林郁芹

Yu-Cin Lin

指導教授：胡振國 博士

Advisor: Jenn-Gwo Hwu, Ph.D.

中華民國 112 年 6 月

June 2023

doi: 10.6342/NTU202300777

國立臺灣大學碩士學位論文
口試委員會審定書
MASTER'S THESIS ACCEPTANCE CERTIFICATE
NATIONAL TAIWAN UNIVERSITY

同心圓金氧半穿隧二極體耦合效應在光傳感中的應用

Applications of Concentric MIS(p) Tunnel Diode Coupling Effect on Photo Sensing

本論文係 林郁芹（R10943070）在國立臺灣大學電子工程學研究所完成之碩士學位論文，於民國 112 年 6 月 9 日承下列考試委員審查通過及口試及格，特此證明。

The undersigned, appointed by the Department / Institute of Electronics Engineering on 9 (date) 6 (month) 2023 (year) have examined a Master's thesis entitled above presented by Yu-Cin Lin (R10943070) candidate and hereby certify that it is worthy of acceptance.

口試委員 Oral examination committee:

胡振國　吳幼麟　胡院令

（指導教授 Advisor）

系主任/所長 Director: 江介宏

`

誌謝

在完成這篇碩士論文之際，我想向所有在過程中給予我支持、指導和鼓勵的人致以最誠摯的感謝。

首先，我衷心地感謝我的指導教授胡振國老師。在整個研究過程中，您耐心解答我的問題，引導我找到研究的方向。您對我的研究提供的寶貴指導和專業建議讓我能更深入理解研究領域，您豐富的經驗對我的學術成長至關重要，能夠成為您的學生，我感到非常榮幸。我還要感謝兩位口試委員吳幼麟教授以及胡璧合教授在百忙之中對我論文的評閱和建議，您們的寶貴意見使我的研究更加完整。

同樣，我要感謝實驗室的所有夥伴以及學長姐。特別要感謝林冠文、陳冠竹、陳人豪、林建宇、黃崧瑋、林津丞、林俊諭以及林彥瑜等學長姐們。在我剛進入實驗室時，你們在實驗操作和數據收集方面給予了我巨大的協助。同時，也非常感謝你們提供的寶貴建議和經驗，並且願意聆聽我的想法和疑問給予我新的思路，使得我的研究能夠順利進行。也非常感謝高綺憶、沈祐德、陳舜啓以及林軒毅等同屆夥伴們，你們的陪伴為我的研究生涯增添了樂趣，與你們在無塵室及量測室的奮鬥時光，是我珍貴的回憶之一。

最後，我要感謝我的家人。感謝您們在我整個求學過程中給予我無限的支持和鼓勵，成為我最堅強的後盾。在我最低落的時候，您們的陪伴總是給予我力量和勇氣，讓我相信自己能夠克服挑戰。您們為我提供良好的學習環境，讓我在生活中無後顧之憂，我真的感到無比幸運和感激。

再次感謝所有人的支持和幫助，使我能夠完成這篇碩士論文。我將永遠珍惜這段獨一無二的經歷。

2023.06.13

林郁芹

doi: 10.6342/NTU20230077

`

摘要

本篇論文主要探討同心圓金氧半穿隧二極體兩鄰近電極間的耦合效應以及耦合效應在光感測方面的影響及其應用。我們探討了一般元件以及去除邊緣氧化層之元件的特性差異，並利用短路電流量測證明耦合效應的存在，也觀察到在不同的閘極偏壓下，有不同的耦合效應機制，對元件電流造成的變化也不同。在累積區的耦合效應是由電子濃度梯度形成的擴散電流主導，而在深空乏區為邊緣電場所造成的電流來主導。其中，去除邊緣氧化物的元件在深空乏區由於邊緣電場分布較窄而缺乏耦合效應。

另外，以量測短路電流作為光感測的參數可以保持較好的線性度為動機，將內圓閘極施加正偏壓，一般元件的外環短路電流可以線性地隨著光強度增加由負增加到正，這種利用耦合效應由負切換到正的現象對於光感測辨識的靈敏度是很大的優勢；至於去除邊緣氧化層的元件，我們發現量測基板電流可以得到暗電流以內圓電流為主導、光電流以外環電流為主導的高光暗電流比。最後，除了短路電流量測，還提出了將基板浮動的特殊操作，藉由這種方式得到在正偏壓下以及負偏壓下都可以操作的光感測方式。相信本篇論文的分析對於光感測發展有其重要性。

關鍵詞：金氧半穿隧二極體、耦合效應、邊緣電場、光感測器、短路電流、線性度、浮動基板

doi: 10.6342/NTU20230077

`

Abstract

This thesis explores the coupling effect between two neighboring electrodes of the concentric MIS(p) tunnel diode and its impact on photo sensing. Specifically, we discuss the differences between general devices and devices with edge-removed oxide and demonstrate the existence of the coupling effect through short-circuit current. The coupling effect is dominated by distinct mechanisms in different regions. In the accumulation region, the diffusion current formed by the electron concentration gradient is the dominant mechanism, while in the deep depletion region, the fringe field dominates. However, devices with edge-removed oxide lack coupling effects in the deep depletion region due to the narrower fringing field distribution.

In addition, using short-circuit current as the photo sensing parameter can maintain good linearity. By applying a positive bias to the inner gate, the short-circuit current of a general outer ring device increases linearly from negative to positive with increasing light intensity. This variable current polarity due to coupling effects provides a notable sensitivity advantage. As for the devices with edge-removed oxide, measuring the substrate current can obtain a higher light-to-dark current ratio, because the photocurrent is dominated by the outer ring, and the dark current is dominated by the inner center. Additionally, we perform a special operation of substrate floating that enables our photo sensing can operate under both positive and negative bias voltages. It is believed that the analysis of

doi: 10.6342/NTU20230077

`

this thesis has important implications for the development of photo sensing.

Key words: MIS tunnel diodes, coupling effect, fringing field, photo sensor, short-circuit current, linearity, floating substrate

doi: 10.6342/NTU20230077

Contents

口試委員會審定書 I

誌謝 II

摘要 III

Abstract IV

Contents VI

Figure Captions VIII

Chapter 1 Introduction 1

1-1 Motivation and Thesis Organization 2

1-2 Co-Planar and Edge-Removed Oxides 3

1-3 *I-V* Characteristics of MIS(p) Tunnel Diodes 4

1-3-1 Effect of Oxide Thickness 5

1-3-2 Fringing Field Effect 6

1-4 MIS(p) Tunnel Diodes for Photodetection 7

1-5 Photo Sensing Parameters 9

1-6 Summary 12

Chapter 2 Lateral Coupling Effect in Concentric MIS(p) Structure 21

2-1 Introduction 22

2-2 Experimental 22

2-3 Results and Discussion 23

2-3-1 Analysis of Coupling Effect by Short Circuit Current 23

doi: 10.6342/NTU20230077

2-3-2 Co-Planar Oxide 24
2-3-3 Edge-Removed Oxide 26
2-4 Summary 27
Chapter 3 Photo Sensing in Concentric Devices 35
3-1 Introduction 36
3-2 Short-Circuit Operation of Co-Planar Oxide 36
3-2-1 Current Polarity Changeable 36
3-2-2 Linear Photodetectivity 37
3-2-3 Power Consumption 38
3-3 Short-Circuit Operation of Edge-Removed Oxide Devices 39
3-3-1 Negligible Dark Current 39
3-3-2 Substrate Current Depending on Device Size 40
3-4 Substrate Floating Operation 41
3-5 Summary 44
Chapter 4 Conclusion and Future Work 61
4-1 Conclusion 62
4-2 Future Work 64
4-2-1 Experimental Limits 64
4-2-2 Effect of Device Size 64
4-2-3 Effect of Gap Oxide Thickness 65
References 69

doi: 10.6342/NTU20230077

`

Figure Captions

Fig. 1-1. The schematic cross sections of MIS(p) TD structures for (a) CP-OX and (b) ER-OX.....13

Fig. 1-2. Typical *I-V* curves of MIS(p) TDs with CP-OX and ER-OX. The directions of the current flow are marked as (+)(-). The thickness of the oxide layer for both devices is about 2.4 nm.....13

Fig. 1-3. *I-V* curves of MIS(p) TDs with various oxide thicknesses for (a) CP-OX and (b) ER-OX. The top insets are the band diagrams of the device edge for both categories. The reverse saturation current increases with oxide thickness for CP-OX due to Schottky barrier height modulation, but is independent of oxide thickness for ER-OX due to the edge leakage paths [9].....14

Fig. 1-4. Schematic of the fringe fields for (a) CP-OX and (b) ER-OX under positive bias. The light orange regions represent the depletion regions. The fringing field is indicated by the red arrow. In the CP-OX case, the electric field extends outward, while in the ER-OX case, the electric field is larger but narrower.....15

Fig. 1-5. *I-V* curves of MIS(p) TDs (a) with and (b) without the neighboring outer gate. It is demonstrated that with a neighboring outer gate, photo response can be effectively enhanced by the proper gate bias [13].....16

Fig. 1-6. Open-circuit voltage with different inner gate biases under varying light intensities. It demonstrated the non-linear response between V_{OC} and Φ.....17

Fig. 1-7. *I-V* curves of MIS(p) TDs with CP-OX and ER-OX under varying light intensities. Inner center is referred to as the drain, while outer rings are represented by G_1 and

doi: 10.6342/NTU20230077

`

G_2, with the numbers indicating the number of rings. It is shown that the light-to-dark current ratio in the case of ER-OX is larger than in the case of CP-OX due to lower reverse saturation current [16].....17

Fig. 1-8. *I-V* curves of the single ring device under varying light intensities. The direction of the current is marked as (+)(-). The current corresponding to zero bias is denoted as I_{SC}, and the voltage at the near-zero point of the current is referred to as V_{OC}.....18

Fig. 1-9. (a) The measurement data and fitting curves of I_{SC} and V_{OC} of the single ring device and (b) Logarithm relationship plot between V_{OC} and I_{SC} under varying light intensities.....19

Fig. 2-1. The schematic diagrams of the top view for (a) single MIS(p) TD and (b) concentric MIS(p) TD. The corresponding cross-sectional schematic diagrams of MIS(p) TDs with CP-OX are shown in (c) and (d), and ER-OX in (e) and (f), respectively.....28

Fig. 2-2. *I-V* curves of (a) CP-OX and (b) ER-OX ring device w/ and w/o gate in the dark. The directions of the current flow are marked as (+)(-). I_{SC} without a gate is near zero, and I_{SC} with -0.4 V gate bias is positive due to the coupling effect. Notably, when using a gate bias of 0.4 V, I_{SC} is negative for the CP-OX device, but almost zero for the ER-OX device. The results suggest that the coupling effects of each concentric device operate through different mechanisms.....29

Fig. 2-3. (a) The current at three terminals of the CP-OX concentric device versus the inner gate voltage. The directions of the current flow are marked (+)(-) by the corresponding color. The inset defines the current directions at the three terminals. Schematic diagram of the coupling mechanism of concentric devices under (b) Region 1: $V_G < V_{FB}$, (c) Region 2: 0 V > $V_G > V_{FB}$, and (d) Region 3: $V_G > 0$ V. The depletion regions are depicted

doi: 10.6342/NTU20230077

in light orange, fringing fields are represented by red arrows, and electrons are depicted in green circles. The green and blue arrows represent the electron and hole currents, respectively.....31

Fig. 2-4. (a) The current at three terminals of the ER-OX concentric device versus the inner gate voltage. The directions of the current flow are marked (+)(-) by the corresponding color. The inset defines the current directions at the three terminals. Schematic diagram of the coupling mechanism of concentric devices under (b) Region 1: $V_G < V_{FB}$, (c) Region 2: 0 V > $V_G > V_{FB}$, and (d) Region 3: $V_G > 0$ V. The depletion regions are depicted in light orange, fringing fields are represented by red arrows, and electrons are depicted in green circles. The green and blue arrows represent the electron and hole currents, respectively.....33

Fig. 3-1. (a) The short-circuit current of the CP-OX outer ring versus the inner gate voltage and the *I-t* diagrams switching between light and dark conditions per second at (b) $V_G = 0$ V and (c) $V_G = 0.4$ V under varying light intensities.....46

Fig. 3-2. (a) The short-circuit current (I_{SC}) of different inner gate biases (V_G) under varying light intensities (Φ). The linear range occurs when the light intensity is greater than 100 lux. The slope of the fitted curve is also indicated. (b) Light intensity threshold (Φ_{th}) for current polarity changes under different inner gate biases (V_G). The thresholds for each bias were predicted from linear relationships.....47

Fig. 3-3. Schematic diagram of the fringing field under illumination. The fringing fields are indicated by red arrows. The yellow circles represent the additional photogenerated electrons. The light orange area indicates the depletion region in the dark, while the dashed yellow line indicates the depletion region boundary that contracts inward under illumination.....48

doi: 10.6342/NTU20230077

Fig. 3-4. (a) I_G-V_G curves with the CP-OX outer ring biased at 0 V under varying light intensities. (b) Power consumption at different gate biases obtained from (a).....49

Fig. 3-5. (a) The short-circuit current of the ER-OX outer ring versus the inner gate voltage under varying light intensities. Due to the absence of coupling effects, the short-circuit current at positive bias is similar to that of a single device.....50

Fig. 3-6. The short-circuit current (I_{SC}) of the ER-OX outer ring under different inner gate biases (V_G) versus varying light intensities (Φ). The concentric device senses the same short-circuit current as a single device regardless of the inner gate positive bias.....50

Fig. 3-7. The current at three terminals of the ER-OX concentric device versus the inner gate voltage (a) in the dark and (b) at the light intensity of 50 lux. The substrate current is dominated by the inner gate in the dark and by the outer ring under illumination.....51

Fig. 3-8. (a) $I_{substrate}$-V_G curves of ER-OX concentric devices with different inner circle radii but the fixed outer radius of the outer ring under dark and illuminated conditions. The photocurrents of the four curves in the positive bias region almost overlap. (b) Substrate current shown in (a) divided by the perimeter of the corresponding inner gate versus inner gate voltage. The dark currents of the four curves in the positive bias region coincide.....52

Fig. 3-9. (a) $I_{substrate}$-V_G curves of ER-OX concentric devices with different outer radii of the outer ring but fixed inner circle radius under dark and illuminated conditions. The dark currents of the three curves in the positive bias region coincide. (b) Substrate current shown in (a) divided by the outer perimeter of the corresponding outer ring versus the inner gate voltage. The photocurrents of the three curves in the positive bias region almost overlap.....53

doi: 10.6342/NTU20230077

Fig. 3-10. (a) I_{Ring}-V_{Ring} curves of substrate floating and inner center grounded, (b) I_{Ring}-V_{Ring} curves of substrate and inner center both grounded, and (c) I_{Center}-V_{Center} curves of substrate and outer ring both grounded under varying light intensities for CP-OX. The saturation current value in the positive voltage region of graph (a) is consistent with that of graph (b), while the saturation current value in the negative voltage region of graph (a) is consistent with that in the positive voltage region of graph (c).....55

Fig. 3-11. (a) Overlay of Figs. 3-10(a) and (b). (b) Overlay of Figs. 3-10(a) and (c).....56

Fig. 3-12. (a) I_{Ring}-V_{Ring} curves of substrate floating and inner center grounded, (b) I_{Ring}-V_{Ring} curves of substrate and inner center both grounded, and (c) I_{Center}-V_{Center} curves of substrate and outer ring both grounded under varying light intensities for ER-OX. The saturation current value in the positive voltage region of graph (a) is consistent with that of graph (b), while the saturation current value in the negative voltage region of graph (a) is consistent with that in the positive voltage region of graph (c).....58

Fig. 3-13. (a) Overlay of Figs. 3-12(a) and (b). (b) Overlay of Figs. 3-12(a) and (c).....59

Fig. 3-14. Substrate-induced voltage versus the outer ring voltage in the dark and at the light intensity of 300 lux.....60

Fig. 4-1. *I-V* curves of concentric center, single center, single ring MIS(p) TDs with different gap oxide thickness. The four graphs are (a) edge-removed oxide (ER-OX), (b) thinner gap oxide, (c) co-planar oxide (CP-OX), and (d) thicker gap oxide. The insets are schematic diagrams of the structure.....68

doi: 10.6342/NTU20230077

`

Chapter 1
Introduction

1-1 Motivation and Thesis Organization

1-2 Co-Planar and Edge-Removed Oxides

1-3 *I-V* Characteristics of MIS(p) Tunnel Diodes

1-3-1 Effect of Oxide Thickness

1-3-2 Fringing Field Effect

1-4 MIS(p) Tunnel Diodes for Photodetection

1-5 Photo Sensing Parameters

1-6 Summary

doi: 10.6342/NTU20230077

`

1-1 Motivation and Thesis Organization

With the advancement of technology, ambient light sensors are prevalent in various aspects of our daily lives, such as smartphones [1], automobiles [2], and LCDs [3]. As a result, there have been many issues associated with ambient light sensors in recent years [4]-[6]. One traditional type of photodetector is the metal-insulator-semiconductor(p) tunnel diode (MIS(p) TD) [7][8]. The MIS(p) structure is named as a tunnel diode due to the quantum tunneling effect of an ultra-thin oxide layer. This device offers many advantages such as simple process flow, low production cost, and high photo sensitivity.

Previous work has proposed that utilizing concentric devices with suitable neighboring gate bias can enhance photosensitivity [13]. Moreover, another previous work has suggested that photosensitivity can be enhanced by using structures that remove the oxide layer at the edge of the device [16]. As a result, this thesis investigates the electrical characteristics and photo sensing applications of two categories of concentric MIS(p) TDs, MIS(p) TD with co-planar oxide (CP-OX) and MIS(p) TD with edge-removed oxide (ER-OX).

This chapter introduces the fundamental *I-V* characteristics of two categories of MIS(p) TDs and discusses relevant previous studies on photo sensing. In addition, this chapter also compares the pros and cons of using open-circuit voltage and short-circuit current as photo sensing parameters, providing the motivation for this thesis to study on

doi: 10.6342/NTU20230077

`

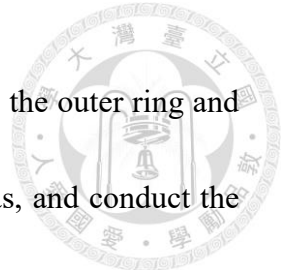

short-circuit current of concentric MIS(p) TDs. In Chapter 2, we bias the outer ring and substrate at 0 V, i.e., short-circuit operation, sweep the inner gate bias, and conduct the analysis of the current at each terminal of the concentric devices. We investigate the coupling effect between two neighboring electrodes by using the characteristic of a near-zero short-circuit current in single MIS(p) TDs. The results show a significant difference in the coupling effect of neighboring electrodes between the two categories of concentric MIS(p) TDs. Next, we explore the applications and phenomena of these two categories in photo sensing using short-circuit current as a measurement parameter in Chapter 3. In addition to the short-circuit operation, a special operation, the floating substrate operation, is also presented in the same chapter. Finally, in Chapter 4, the experimental limitation of this thesis is mentioned and future work directions are proposed, including optimizing the photo sensing performance of the device and investigating other categories of MIS(p) TD structures.

1-2 Co-Planar and Edge-Removed Oxides

The previous work [9] introduced two categories of MIS(p) structures. The first category is MIS(p) with coplanar oxide (CP-OX), which has a complete SiO_2 layer on a silicon substrate. The second category is MIS(p) with edge-removed oxide (ER-OX), which is characterized by only a SiO_2 layer between the silicon substrate and the top aluminum electrode, as shown in Fig. 1-1. These two structures have distinctly different

doi: 10.6342/NTU20230077

`

electrical characteristics in the deep depletion region. The current of the CP-OX structure is modulated by the Schottky barrier height [7], whereas the current of the ER-OX structure is influenced by the edge-leakage effect [9]. Therefore, the saturation current of the ER-OX structure is lower than that of the CP-OX structure as shown in Fig. 1-2. The details of these electrical characteristics will be introduced in the next section.

1-3 *I-V* Characteristics of MIS(p) Tunnel Diodes

The MIS(p) structure with an ultra-thin oxide layer exhibits diode-like electrical characteristics and is known as a tunnel diode due to quantum tunneling phenomena. Due to the ideal diode law [10], the current-voltage relationship of a diode is:

$$I = I_0(e^{\frac{qV}{nkT}} - 1) \qquad (1\text{-}1)$$

where I is the current through the diode, V is the voltage across the diode, I_0 is the reverse saturation current, n is the ideality factor, k is the Boltzmann constant, T is the temperature, and q is the charge of an electron.

In the case of CP-OX, the reverse saturation current (I_0) is dominated by the hole current (I_{h}), and it can be described as [11]:

$$I_{\mathrm{h}} = A^* A_{\mathrm{eff}} P_{\mathrm{t}} T^2 e^{\frac{-q\emptyset_{\mathrm{h}}^*}{kT}} \qquad (1\text{-}2)$$

where A^* is the effective Richardson constant, A_{eff} is the effective area for the hole flux, P_{t} is the tunneling probability, $\emptyset_{\mathrm{h}}^*$ is the effective Schottky barrier height for holes.

However, in the case of ER-OX, removing the oxide layer through wet etching

doi: 10.6342/NTU20230077

`

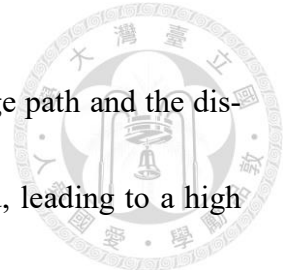

results in defects on the oxide edge. This creates an additional leakage path and the distribution of fringing field under reverse bias is significantly changed, leading to a high tunneling probability. Therefore, the reverse saturation current is dominated by the electron tunneling current [9].

1-3-1 Effect of Oxide Thickness

The *I-V* curves of CP-OX and ER-OX MIS(p) TDs with various oxide thicknesses are shown in Fig. 1-3 [9]. As the oxide thickness reduces, the negative current increases in the negative bias region. The current under negative bias is primarily determined by the tunneling electron flow, and a thinner oxide layer leads to a higher tunneling rate, resulting in increased current in the negative bias region.

Interestingly, these two categories of MIS(p) TDs have different characteristics in the positive bias region. The band diagrams of the device edge for both categories are shown at the top of Fig. 1-3. In the case of CP-OX, as the oxide thickness increases, the saturation current also increases in the deep depletion region. This phenomenon can be explained by the mechanism known as Schottky barrier height modulation. The effective Schottky barrier height $\emptyset_h^*$ can be expressed as the following equation [11]:

$$\emptyset_{\mathrm{h}}^{*} = \chi_{\mathrm{s}} - \Phi_{\mathrm{m}} + \frac{E_{\mathrm{g}}}{q} - V_{\mathrm{ox}} \qquad (1\text{-}3)$$

where χ_{s} is the electron affinity of the semiconductor, Φ_{m} is the work function of the metal, E_{g} is the band gap of the semiconductor, and V_{ox} is the voltage drop across the

doi: 10.6342/NTU20230077

`

oxide layer. A thicker oxide layer reduces the rate of electron tunneling to the metal, which means that less band bending of silicon is required to maintain charge neutrality. This results in more voltage being dropped across the oxide layer. According to Eq. (1-3), a larger oxide voltage drop would cause a lower effective Schottky barrier height. Therefore, a thicker oxide results in a larger hole current.

However, in the case of ER-OX, the tunneling probability is high due to additional leakage paths. The large leakage characteristic of the minority carriers results in a negligible voltage drop across the oxide layer. Therefore, the effective Schottky barrier height cannot be modulated by V_{ox}, the saturation current is irrelevant to the oxide thickness. That is to say, the saturation current is dominated by the electron tunneling current, which is highly influenced by the defect density on the edge oxide.

1-3-2 Fringing Field Effect

The fringing field is an electric field that exists at the edges of the depletion region due to the non-uniform distribution of charges. The depletion region appears when the bias voltage at MIS(p) TD is larger than the flat-band voltage. The high tunneling rate of ultra-thin oxide results in a reduced accumulation of inversion electrons, widening the depletion region that compensates for the leakage of inversion charges. Additionally, in the case of CP-OX, neighboring oxide charges create a lateral extension of the depletion region [12]. Consequently, the lateral fringing field extends outward meanwhile.

doi: 10.6342/NTU20230077

`

The depletion width in the case of ER-OX is wider than in the case of CP-OX due to the high tunneling probability through additional leakage paths. Wider depletion width results in larger fringing field. However, the removal of the surrounding oxide outside of the device means there are no neighboring oxide charges, preventing the depletion region from extending laterally. Therefore, the lateral fringing field cannot extend outward. In conclusion, although the ER-OX device generates larger electric field, the range of fringing field distribution is narrower [9]. The schematic diagrams of the depletion width and electric field distribution for both categories are plotted in Fig. 1-4.

1-4 MIS(p) Tunnel Diodes for Photodetection

At the reverse bias, MIS(p) TD with CP-OX is characterized by a slight change in the effective Schottky barrier height induced by surrounding signals that will significantly change the tunneling current, which means MIS(p) tunnel diode with CP-OX exhibits excellent photosensitivity. In addition, introducing a neighboring gate can significantly impact the current of MIS(p) TD with CP-OX [13]. The concentration of minority carriers strongly influences the deep depletion current, as explained in Section 1-3. Therefore, altering the gate bias to control the minority carrier concentration distribution can modify the current behavior. The sensing results of single and concentric MIS(p) TD with CP-OX are shown in Fig. 1-5 [13]. The results indicate that the dark current of the concentric device significantly reduces when the gate bias is near the flat-band voltage. This is

doi: 10.6342/NTU20230077

`

because the flat-band condition of the neighboring gate limits the supply of minority carriers to the sensing electrode, leading to an increase in the Schottky barrier height. Therefore, the light-to-dark current ratio of the concentric device is higher than the single device.

In addition, it has been proposed that using a concentric device with the inner center as the gate and the outer ring as the sensor (IGOS) has higher sensitivity than the inner center as the sensor and the outer ring as the gate (ISOG) [14]. This is due to the asymmetric coupling effect. A common method for photo sensing is to measure the saturation light-to-dark current ratio. Although concentric devices can provide improved sensitivity compared to single devices, the trade-off is the power consumption of the two electrodes. Thankfully, a novel method for light sensing by measuring open-circuit voltage has been introduced [15]. Since the sensor remains floating during operation, the power consumption is extremely low. However, the open-circuit voltage does not exhibit a linear relationship with light intensity, potentially affecting the accuracy and reliability of the sensor. Photodetection linearity is a crucial property of photodetectors, which indicates the ability of a detector to respond proportionally to light intensity. Fig. 1-6 displays the open-circuit sensing results at varying light intensities for different inner gate biases, indicating not only a non-linear response but also voltage saturation at higher levels of light intensity. This phenomenon will be explained in the next section.

doi: 10.6342/NTU20230077

`

In addition to introducing the neighboring gate, previous work [16] has shown that MIS(p) TD with ER-OX has a higher light-to-dark current ratio compared to MIS(p) TD with CP-OX due to the lower reverse saturation current observed in MIS(p) TD with ER-OX. Fig. 1-7 shows the *I-V* curves of these two categories in the dark and light. This phenomenon is explained in Section 1-3 as a result of edge leakage effects.

1-5 Photo Sensing Parameters

Fig. 1-8 shows the *I-V* curves of the single MIS(p) TD device under different light intensities. The short-circuit current ($I_{\mathrm{SC(w/o\ Gate)}}$) is defined as the current flowing through the ring MIS(p) TD when there is no potential difference present between its two terminals, i.e., $V_{\mathrm{Ring}} = 0$ V. The open-circuit voltage ($V_{\mathrm{OC(w/o\ Gate)}}$) is defined as the potential difference measured between the two terminals of the ring MIS(p) TD when there is no current flowing through, i.e., $I_{\mathrm{Ring}} = 0$ A. In Fig. 1-8 the near-zero point of current can be regarded as the open-circuit point. Generally, both short-circuit current and open-circuit voltage are close to zero in the dark. However, in the case of illumination, incident photons are absorbed to generate electron-hole pairs that are separated by the built-in electric field to produce photocurrent before recombination [17], which is known as the photovoltaic effect. This effect allows us to detect light by measuring the short-circuit current or open-circuit voltage. According to [15], light is sensed by measuring the open-circuit voltage of the floating electrode, resulting in extremely low power consumption.

doi: 10.6342/NTU20230077

`

However, as the illuminance gets larger and larger, the sensing performance of this method decreases. The following paragraphs will explain this phenomenon in detail.

Short-circuit current (I_{SC}) and open-circuit voltage (V_{OC}) are important parameters for analyzing the characteristics of photovoltaic devices. For a p-n junction diode, the relationship between short-circuit current and light irradiance can be described by the following equation [10][18]:

$$I_{\mathrm{ph}} = \frac{qA\eta E_{\mathrm{e}}}{h\nu} \qquad (1\text{-}4)$$

where the photogenerated current, denoted as I_{ph}, can be considered equivalent to I_{SC} as I_{SC} can be ignored in the absence of light., A is the absorption area of the device, η is the quantum efficiency, E_{e} is light irradiance falling on area A, $h\nu$ is the energy of the incident photons. Eq. (1-4) demonstrates that the short-circuit current is proportional to the light irradiance.

Moreover, the relationship between V_{OC} and I_{SC} is obtained as [10][19]:

$$V_{OC} = \frac{nkT}{q}\ln\left(\frac{I_{SC}}{I_0} + 1\right) \qquad (1\text{-}5)$$

where I_0 is the saturation current of the diode, T is the temperature, k is the Boltzmann constant, and n is the ideality factor of the p-n junction diode. It can be known from Eq. (1-5) that if $I_{SC} \gg I_0$, V_{OC} changes with the logarithm of I_{SC}/I_0, which means the value of V_{OC} changes very little when the current ratio changes relatively large. As a result, when the illuminance is high, V_{OC} tends to have a limited value. Taking V_{OC}

doi: 10.6342/NTU20230077

`

as the detection parameter, the photo responsivity will be worse with increasing illuminance.

The characteristics of MIS(p) TD are similar to the p-n junction diode [20][21], so it can be speculated that the above theory is still applicable to MIS(p) TD. To confirm this postulation, we performed experiments. Fig. 1-9(a) shows the measurement data of open-circuit voltage and short-circuit current of MIS(p) TD single ring device without gate under different light intensities. In fact, the linearity of the relationship between light intensity and short-circuit current can be influenced by several factors, including recombination rate, thermal effects, and noise. Nonetheless, the fitting curve indicates that there is a roughly linear relationship between light intensity and short-circuit current, and the relationship between the open-circuit voltage and light intensity is approximately logarithmic. The coefficient of determination for the measured data and two fitting curves are 0.99635 and 0.99969, respectively, indicating a strong correlation. Moreover, Fig. 1-9(b) shows the relationship between V_{OC} and I_{SC}, which is logarithmic as demonstrated by the measured data and fitting curve. The coefficient of determination is 0.99943. The experimental results provide further support for the postulation. Therefore, in this thesis, we study the feasibility of measuring the short-circuit current of concentric devices to achieve good linearity in photo sensing applications.

doi: 10.6342/NTU20230077

`

1-6 Summary

This chapter begins with an overview of the subject structure of this thesis, followed by the introduction of two categories of MIS(p) TD structures and their electrical characteristics. We also discuss previous studies using MIS(p) TDs for photodetection and explain the main reason and motivation for using short-circuit current as a photodetection parameter in this thesis. Building on this basic knowledge, the following two chapters will investigate the coupling effect of concentric MIS(p) TDs and their applications in photodetection.

doi: 10.6342/NTU20230077

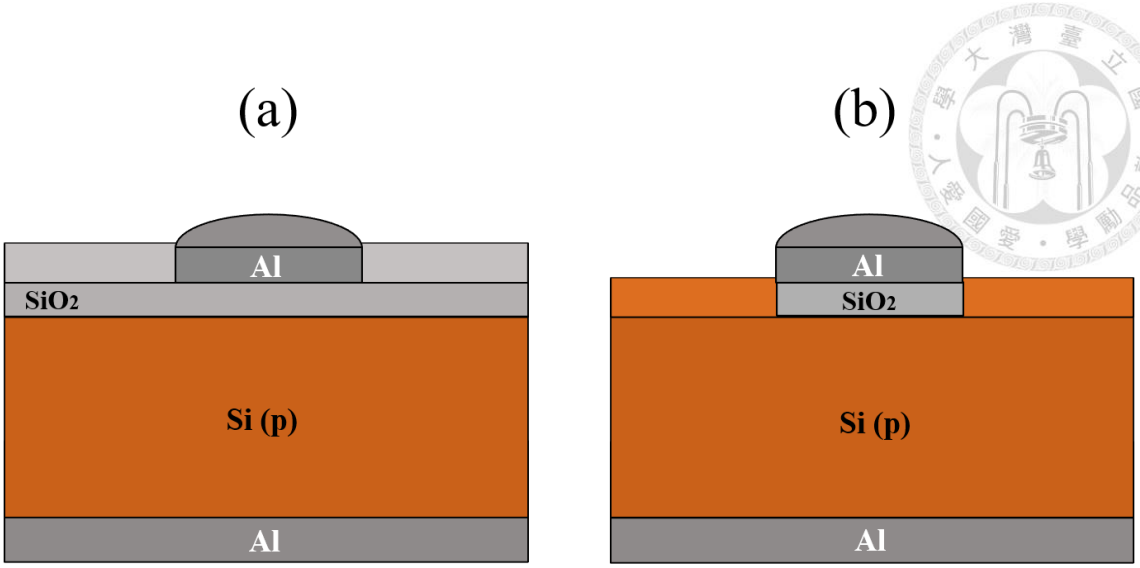

Fig. 1-1. The schematic cross sections of MIS(p) TD structures for (a) CP-OX and (b) ER-OX.

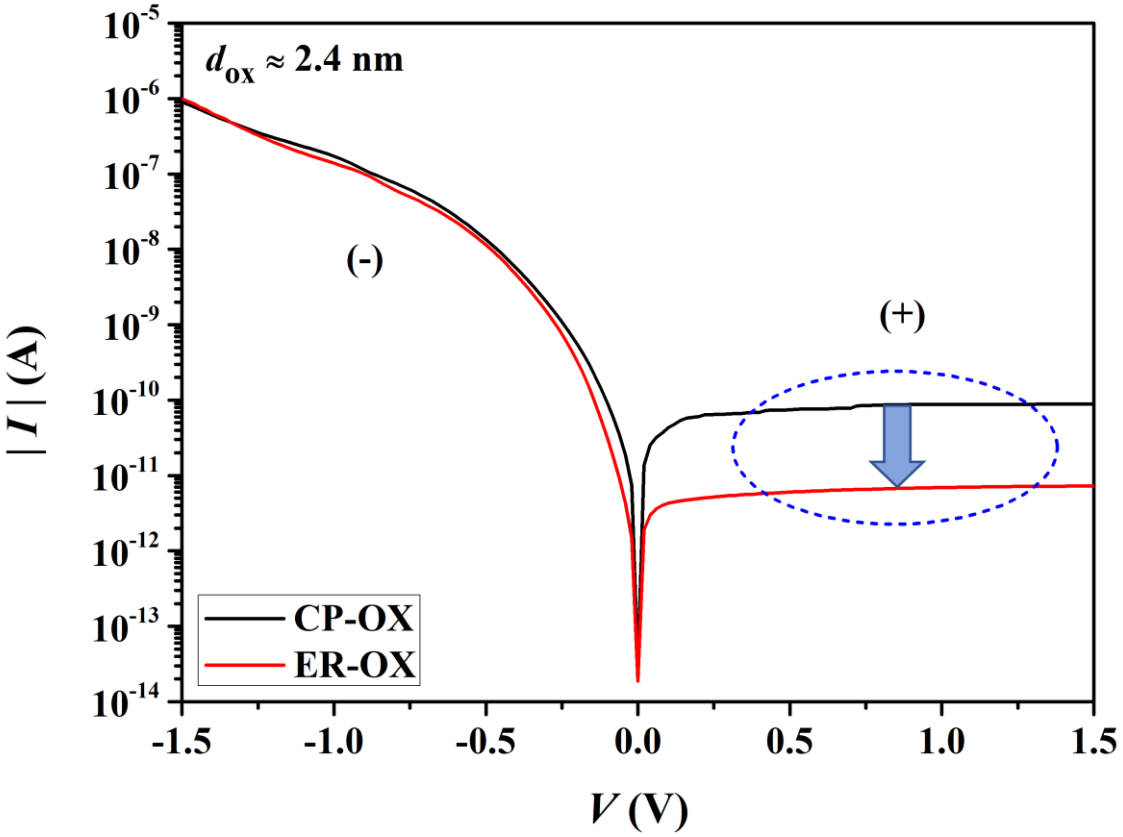

Fig. 1-2. Typical *I-V* curves of MIS(p) TDs with CP-OX and ER-OX. The directions of the current flow are marked as (+)(-). The thickness of the oxide layer for both devices is about 2.4 nm.

doi: 10.6342/NTU20230077

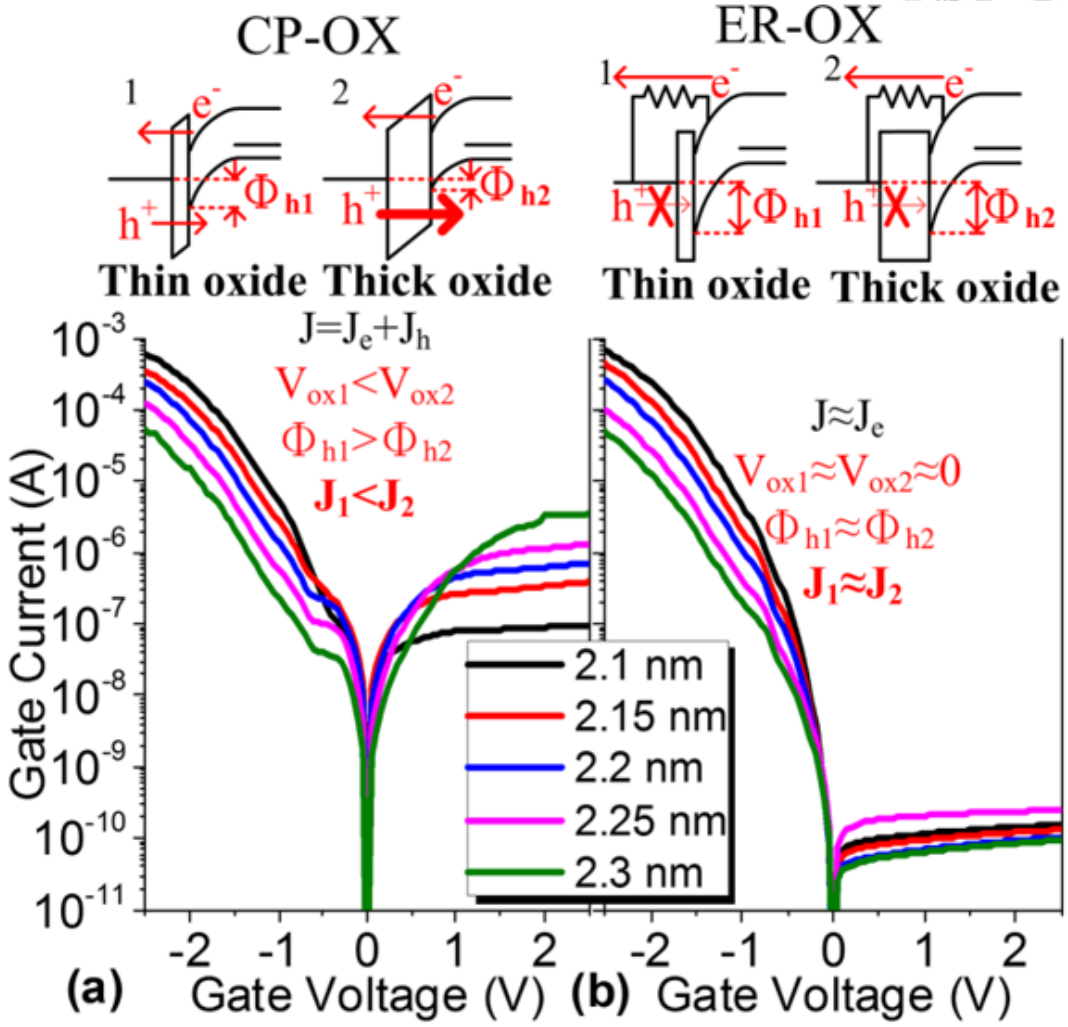

Fig. 1-3. *I-V* curves of MIS(p) TDs with various oxide thicknesses for (a) CP-OX and (b) ER-OX. The top insets are the band diagrams of the device edge for both categories. The reverse saturation current increases with oxide thickness for CP-OX due to Schottky barrier height modulation, but is independent of oxide thickness for ER-OX due to the edge leakage paths [9].

doi: 10.6342/NTU20230077

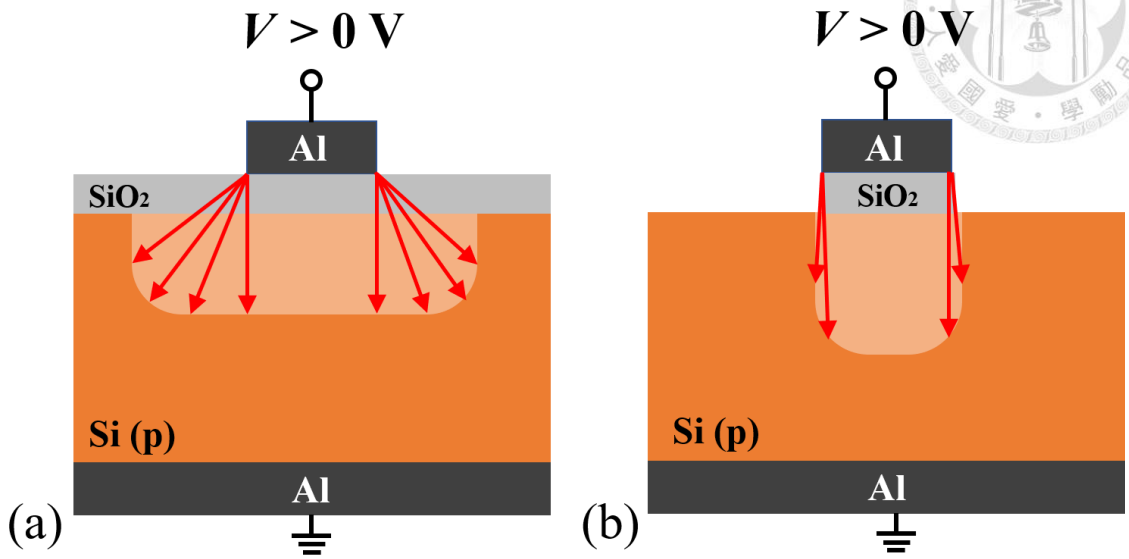

Fig. 1-4. Schematic of the fringe fields for (a) CP-OX and (b) ER-OX under positive bias. The light orange regions represent the depletion regions. The fringing field is indicated by the red arrow. In the CP-OX case, the electric field extends outward, while in the ER-OX case, the electric field is larger but narrower.

doi: 10.6342/NTU20230077

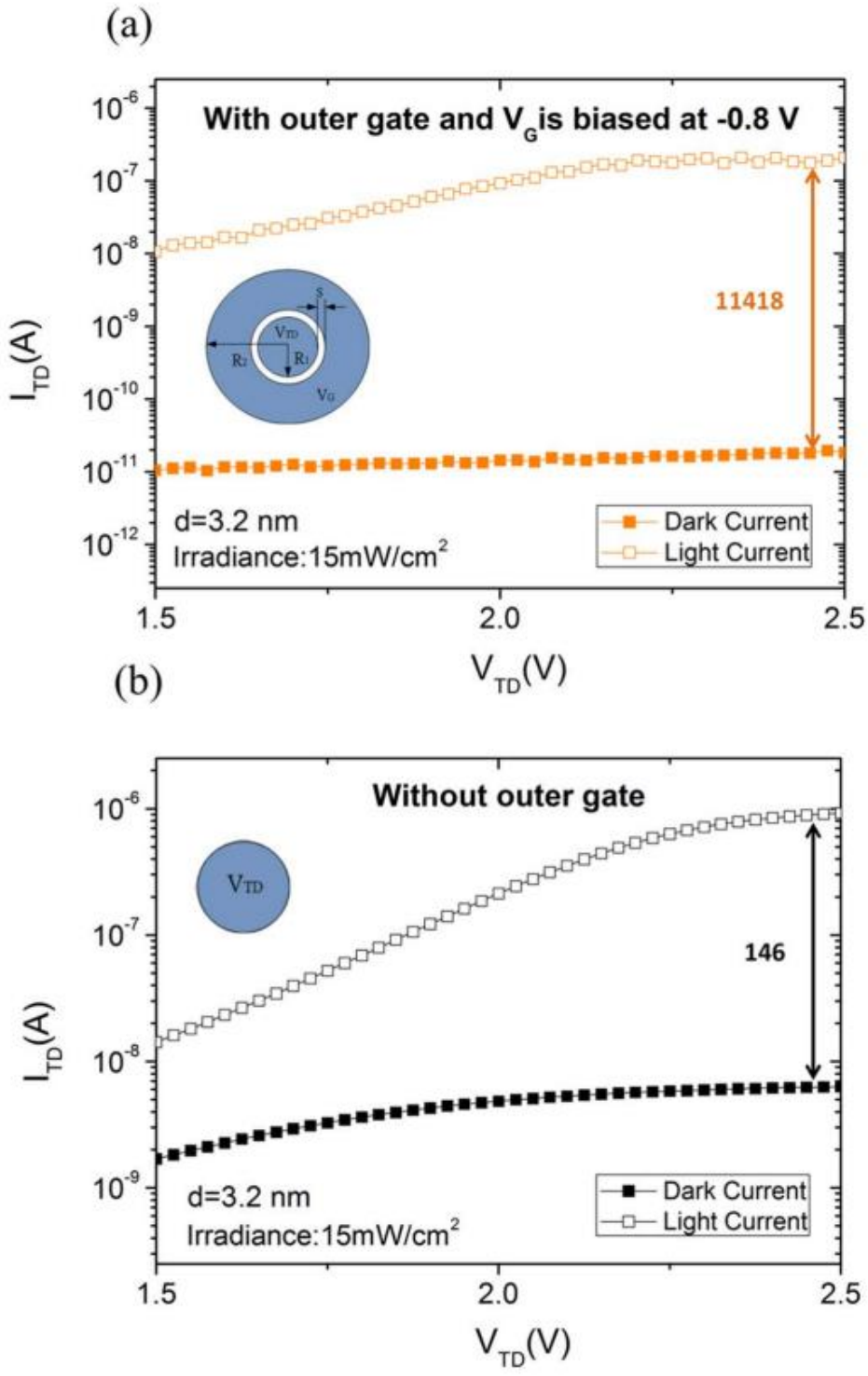

Fig. 1-5. *I-V* curves of MIS(p) TDs (a) with and (b) without the neighboring outer gate. It is demonstrated that with a neighboring outer gate, photo response can be effectively enhanced by the proper gate bias [13].

doi: 10.6342/NTU20230077

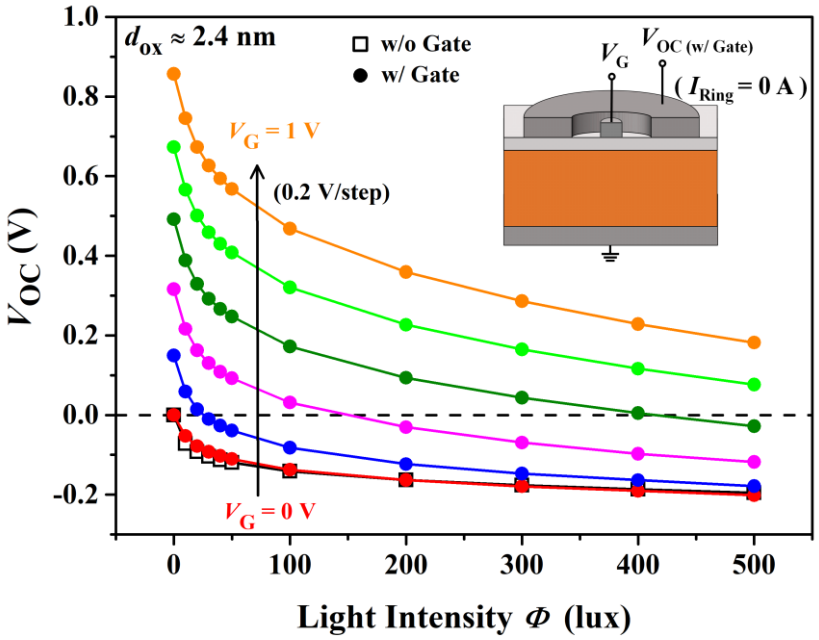

Fig. 1-6. Open-circuit voltage with different inner gate biases under varying light intensities. It demonstrated the non-linear response between V_{OC} and Φ.

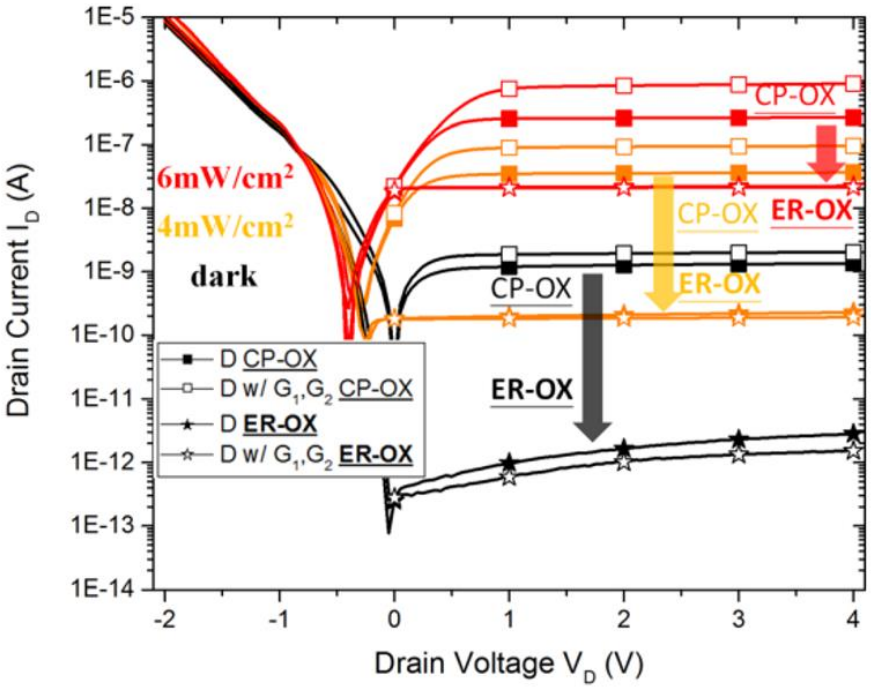

Fig. 1-7. *I-V* curves of MIS(p) TDs with CP-OX and ER-OX under varying light intensities. Inner center is referred to as the drain, while outer rings are represented by G_1 and G_2, with the numbers indicating the number of rings. It is shown that the light-to-dark current ratio in the case of ER-OX is larger than in the case of CP-OX due to lower reverse saturation current [16].

doi: 10.6342/NTU20230077

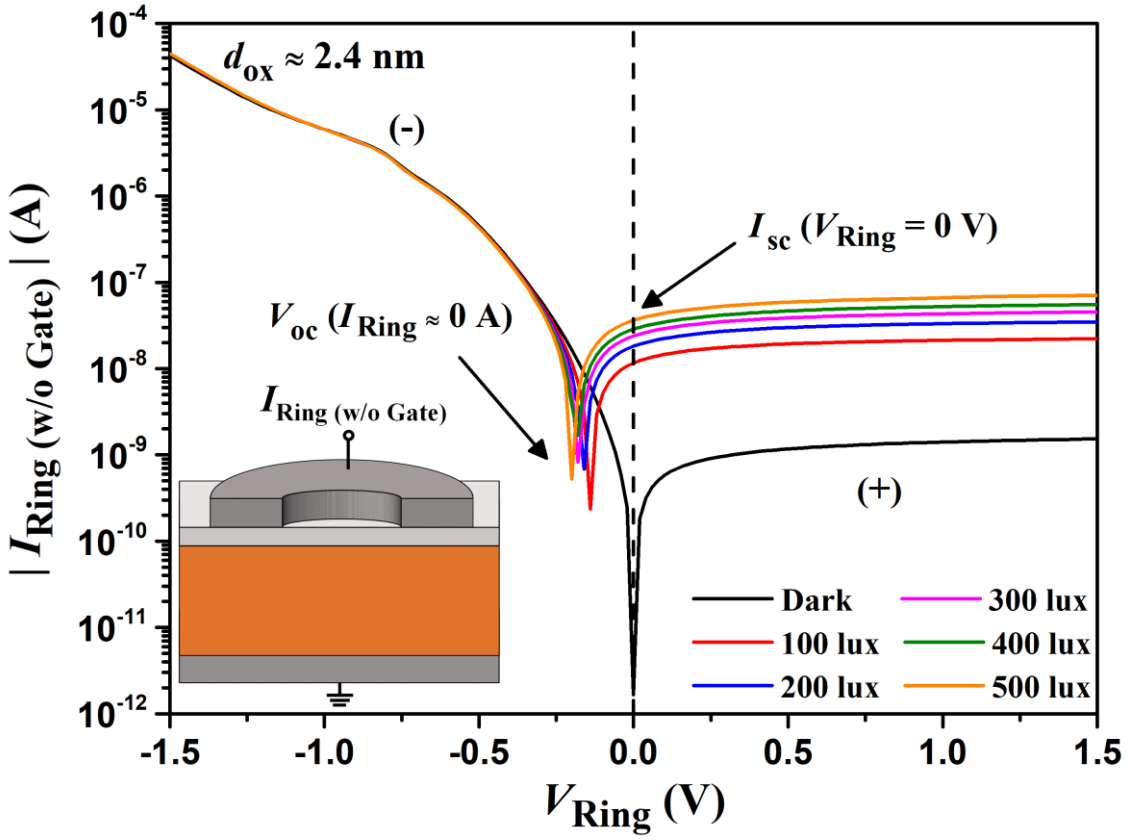

Fig. 1-8. *I-V* curves of the single ring device under varying light intensities. The direction of the current is marked as (+)(-). The current corresponding to zero bias is denoted as I_{SC}, and the voltage at the near-zero point of the current is referred to as V_{OC}.

doi: 10.6342/NTU20230077

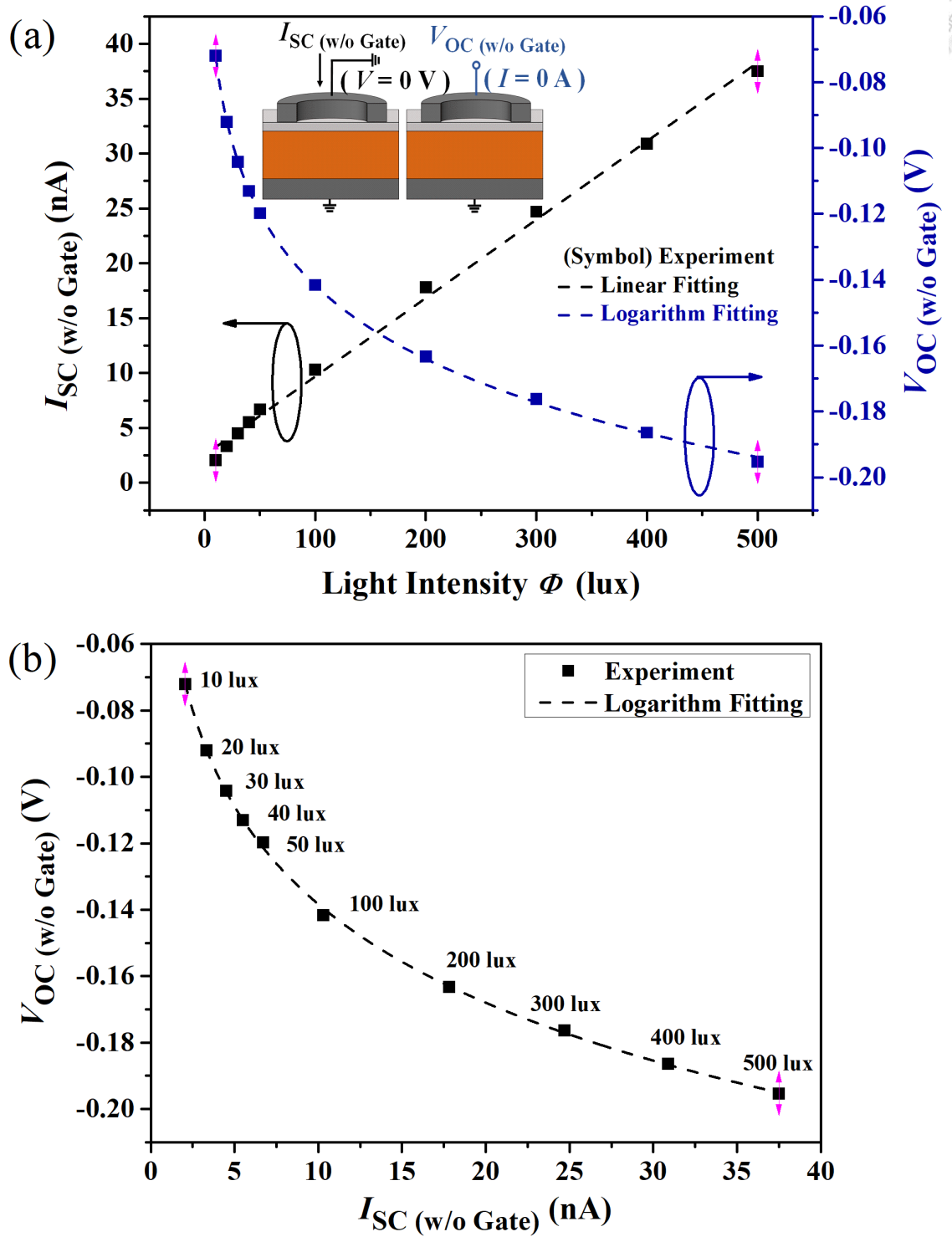

Fig. 1-9. (a) The measurement data and fitting curves of I_{SC} and V_{OC} of the single ring device and (b) Logarithm relationship plot between V_{OC} and I_{SC} under varying light intensities.

doi: 10.6342/NTU20230077

、

doi: 10.6342/NTU20230077

`

Chapter 2
Lateral Coupling Effect in Concentric MIS(p) Structure

2-1 Introduction

2-2 Experimental

2-3 Results and Discussion

2-3-1 Analysis of Coupling Effect by Short Circuit Current

2-3-2 Co-Planar Oxide

2-3-3 Edge-Removed Oxide

2-4 Summary

doi: 10.6342/NTU20230077

`

2-1 Introduction

In Chapter 1, the electrical characteristics of two MIS structures, CP-OX and ER-OX, are compared, and the applications of MIS TDs proposed in the past for light sensing are discussed. One of these applications, the concentric MIS tunnel photodiodes, was found to exhibit higher photosensitivity due to the coupling effect between neighboring electrodes [13]. Furthermore, photosensitivity can be further enhanced by applying an appropriate bias to the neighboring gate. Since gate control is identified as a critical issue in concentric devices, this chapter will focus on the coupling effect in two different categories of MIS tunnel diodes with varying gate biases and discuss the mechanisms behind the resulting coupling effects.

2-2 Experimental

The substrate used was a boron-doped p-type silicon wafer with a resistivity of 1-10 Ω·cm. Surface impurities and native oxide on the surface were eliminated through a Standard Radio Corporation of America (RCA) clean. An ultra-thin silicon dioxide layer with different thicknesses was grown on the tilted wafer by anodization (ANO) system in deionized water at room temperature with a DC voltage of 15 V for 8 minutes. To minimize interface defects, a rapid thermal process was carried out in 20-torr N_2 ambient at 950 ℃ for 15 seconds after the growth of the silicon dioxide layer. A 200-nm thick layer of Al was deposited on top of the oxide layer through thermal evaporation. Then,

doi: 10.6342/NTU20230077

`

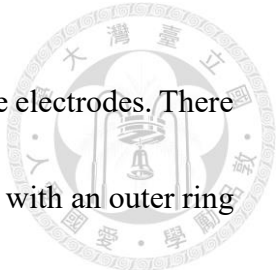

photolithography and wet etching process were carried out to define the electrodes. There are two kinds of device patterns, i.e., single ring and concentric device with an outer ring and inner circle. The inner circle's radius and the outer ring's width are 85 μm and 485 μm, respectively, and the separation between the two electrodes is 30 μm. Their patterns are shown in Figs. 2-1(a) and (b). Next, to form ER-OX, the wafer was dipped into buffered oxide etchant (BOE) to remove the edge oxide. However, for CP-OX, this step was skipped. Finally, after removing the photoresist, the native oxide on the back of the wafer was eliminated by BOE, and a 200-nm thick Al was deposited on the back side as the back contact. The cross-sectional diagrams of MIS(p) TDs with CP-OX are shown in Figs. 2-1(c) and (d), and MIS(p) TDs with ER-OX are shown in Figs. 2-1(e) and (f). The electrical characteristics of these structures were all measured by Agilent B1500A.

2-3 Results and Discussion

All devices mentioned in this section have an oxide layer thickness (d_{ox}) of approximately 2.4 nm.

2-3-1 Analysis of Coupling Effect by Short Circuit Current

In general, when a device is biased at 0 V, the current, i.e., short-circuit current (I_{SC}), is very weak in the dark. Therefore, we analyzed the coupling effect of the concentric device by observing the outer ring short-circuit current variation concerning the effect of inner gate bias. Figs. 2-2(a) and (b) show the *I–V* curves of the CP-OX and ER-OX ring

doi: 10.6342/NTU20230077

`

devices under three conditions: no gate, 0.4 V gate bias, and −0.4 V gate bias in the dark. In the case of CP-OX (Fig. 2-2(a)), the ring device without a gate has a negligible short-circuit current, which is consistent with what was stated in the beginning. However, for the ring device with a gate bias of 0.4 V, the short-circuit current is negative, while for -0.4 V, it is positive. Apparently, when a concentric inner gate is added inside the outer ring, the short-circuit current of the outer ring will have different current behavior under different gate biases due to the coupling effect between two neighboring electrodes. Turning to the case of ER-OX (Fig. 2-2(b)), the ring device without a gate and with a gate bias of -0.4 V exhibits similar short-circuit current behavior to CP-OX, but the short-circuit current is still close to zero at 0.4 V. Obviously, the two MIS TDs with different structures also have different coupling mechanisms. To clarify the coupling effect, the following two subsections will analyze the current at each terminal of the concentric devices.

2-3-2 Co-Planar Oxide

Fig. 2-3(a) demonstrates the current curves for the three terminals of the concentric device with CP-OX. The back electrode and the outer ring are biased at 0 V, allowing for short-circuit operation, and the inner gate bias is swept from -1.5 V to 1.5 V. It is observed that when the inner gate is negatively biased, the short-circuit current of the outer ring is not weak. Fig. 2-3(b) illustrates that a great amount of electrons tunnel from the metal to the substrate when $V_G < V_{FB}$ (about -0.9 V). Although most of the electron flow toward

doi: 10.6342/NTU20230077

`

the back electrode, a small amount diffuses toward the neighboring outer ring owing to the concentration gradient. The insets of schematic electron concentration (n_e) versus distance (x) between the inner gate and outer ring are also depicted in Fig. 2-3(b).

When the gate bias exceeds the flat-band voltage (-0.9 V < V_G < 0 V), the number of tunneling electrons decreases, as depicted in Fig. 2-3(c). Furthermore, due to the reversal of the electric field direction at the Si/SiO_2 interface, some inversion electrons tunnel toward the metal gate. With a reduction in the number of electrons under the inner gate, the slope of the electron concentration gradient also decreases, as illustrated in the insets of Fig. 2-3(c). Notably, the vertical electric field between the inner gate and back electrode diminishes, allowing the lateral fringing field under the outer ring to compete with the vertical electric field for electrons. This implies that, when the vertical electric field is weaker than the lateral fringing field, a greater number of electrons flow from the inner gate to the outer ring. As a result, in this region, the coupling effect between the outer ring and the inner gate is caused not only by the diffusion current but also by the fringe field.

Fig. 2-3(d) depicts the case in which the gate bias is positive (V_G > 0 V). The high tunneling rate of the ultra-thin oxide prevents the electrons from accumulating in the inversion layer, resulting in the widening of the depletion region and outward extension of the fringing field. Moreover, the lateral fringing field causes the hole current of the inner gate to couple with the outer ring, leading to a negative short-circuit current of the outer

doi: 10.6342/NTU20230077

`

ring in the deep depletion region. The curve of short-circuit current merges with the curve of gate current, as shown in region 3 of Fig. 2-3(a).

2-3-3 Edge-Removed Oxide

Fig. 2-4(a) demonstrates the current curves for the three terminals of the concentric device with ER-OX. The back electrode and the outer ring are biased at 0 V, allowing for short-circuit operation, and the inner gate bias is swept from -1.5 V to 1.5 V. It is observed that when $V_G < V_{FB}$ (about -0.9 V) the current behavior is similar to CP-OX. Fig. 2-4(b) also illustrates the same situation with the CP-OX case. The coupling effect between the inner gate and outer ring is dominated by the electrons concentration gradient which is shown in the insets of Fig. 2-4(b).

Fig. 2-4(c) shows the case where the gate voltage is between the flat-band voltage and 0 V (-0.9 V < V_G < 0 V). Due to the narrower fringe field beneath the outer ring, it cannot compete with the vertical electric field between the inner gate and back electrode for electrons. As a result, most of the electrons flow toward the back electrode, and only a small number of electrons below the inner gate are influenced by the concentration gradient and flow toward the outer ring. The schematic electron concentration gradient insets are also shown in Fig. 2-4(c). In this region, the coupling effect between the outer ring and the inner gate is only caused by the electron concentration gradient, which differs from the CP-OX case.

doi: 10.6342/NTU20230077

`

Fig. 2-4(d) demonstrates a significant difference in the case of a positive bias applied to the inner gate ($V_G > 0$ V) compared to the CP-OX case. Due to the positive bias applied to the inner gate, there is a lack of a large number of tunneling electrons to form a diffusion current, and due to the narrower fringing field distribution, the current cannot flow toward the outer ring through the fringe field as in the case of CP-OX. Therefore, as shown in Fig. 2-4(a), the short-circuit current of the outer ring is almost negligible in the deep depletion region, indicating that there is no coupling effect.

2-4 Summary

In this chapter, we analyze the concentric MIS TDs coupling effect by inner gate biasing and outer ring short-circuit operation. The results of two categories (CP-OX/ER-OX) are compared and the dominant factors in the coupling effect are discussed. The diffusion current dominates in the accumulation region, while the fringing field dominates in the deep depletion region. The distribution of fringe fields is responsible for the significant difference in the coupling effect of neighboring electrodes between the case of CP-OX and ER-OX. In the deep depletion region, the short-circuit current of the CP-OX outer ring is negative due to the lateral stretch-out fringing field. However, the short-circuit current of the ER-OX outer ring is near zero because the narrower fringing field results in no coupling effect between the inner gate and the outer ring.

doi: 10.6342/NTU20230077

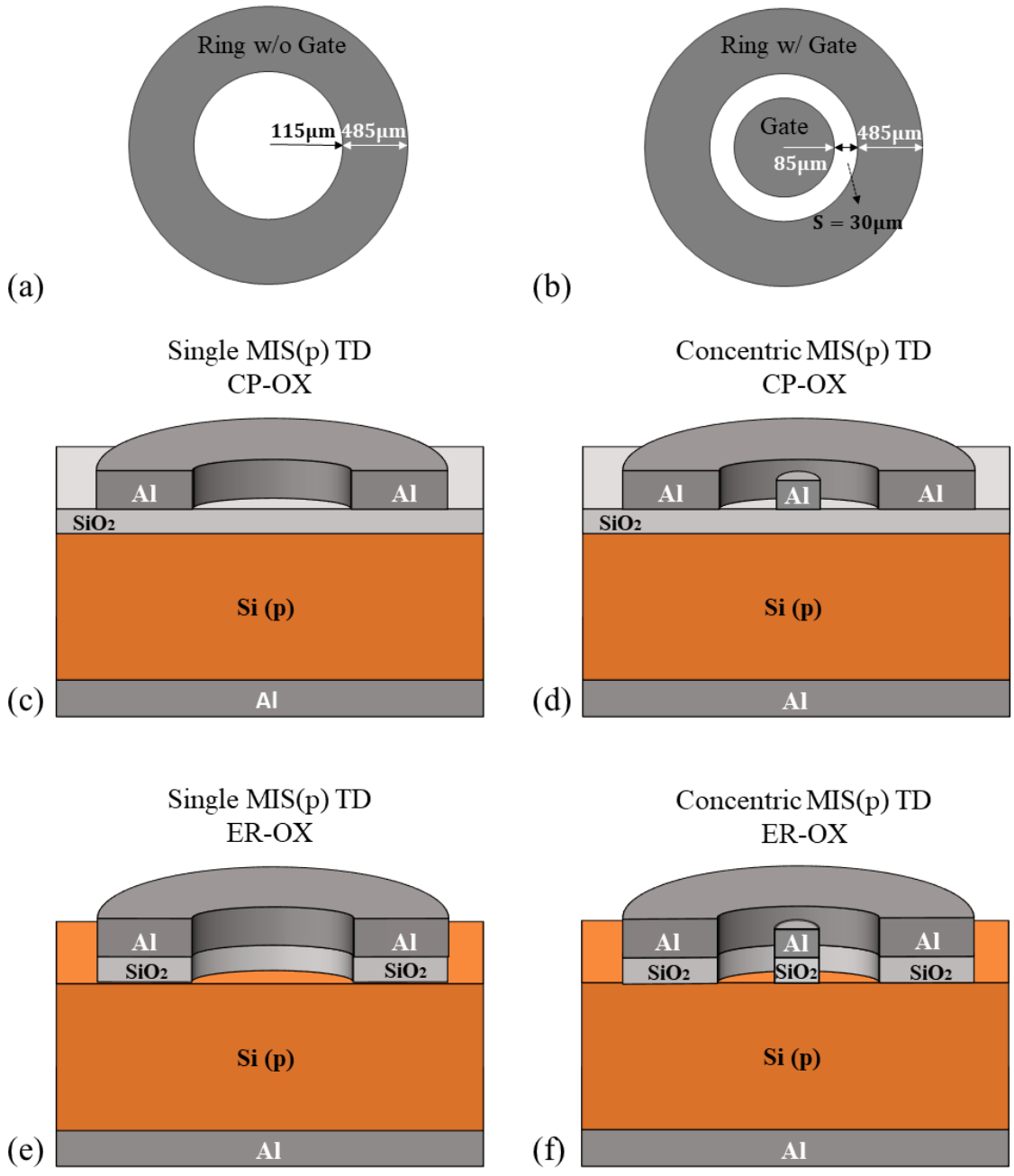

Fig. 2-1. The schematic diagrams of the top view for (a) single MIS(p) TD and (b) concentric MIS(p) TD. The corresponding cross-sectional schematic diagrams of MIS(p) TDs with CP-OX are shown in (c) and (d), and ER-OX in (e) and (f), respectively.

doi: 10.6342/NTU20230077

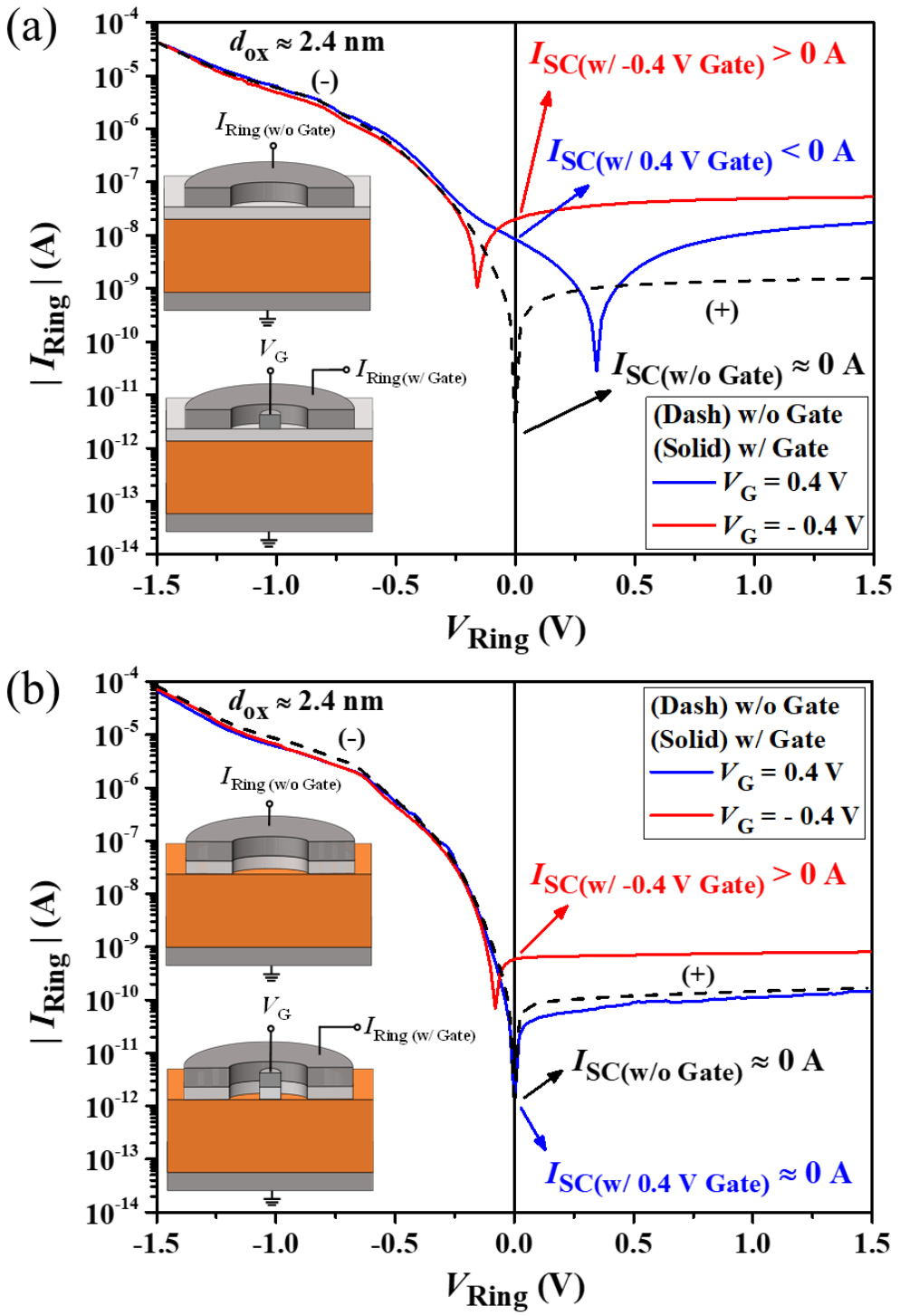

Fig. 2-2. *I-V* curves of (a) CP-OX and (b) ER-OX ring device w/ and w/o gate in the dark. The directions of the current flow are marked as (+)(-). I_{SC} without a gate is near zero, and I_{SC} with -0.4 V gate bias is positive due to the coupling effect. Notably, when using a gate bias of 0.4 V, I_{SC} is negative for the CP-OX device, but almost zero for the ER-OX device. The results suggest that the coupling effects of each concentric device operate through different mechanisms.

doi: 10.6342/NTU20230077

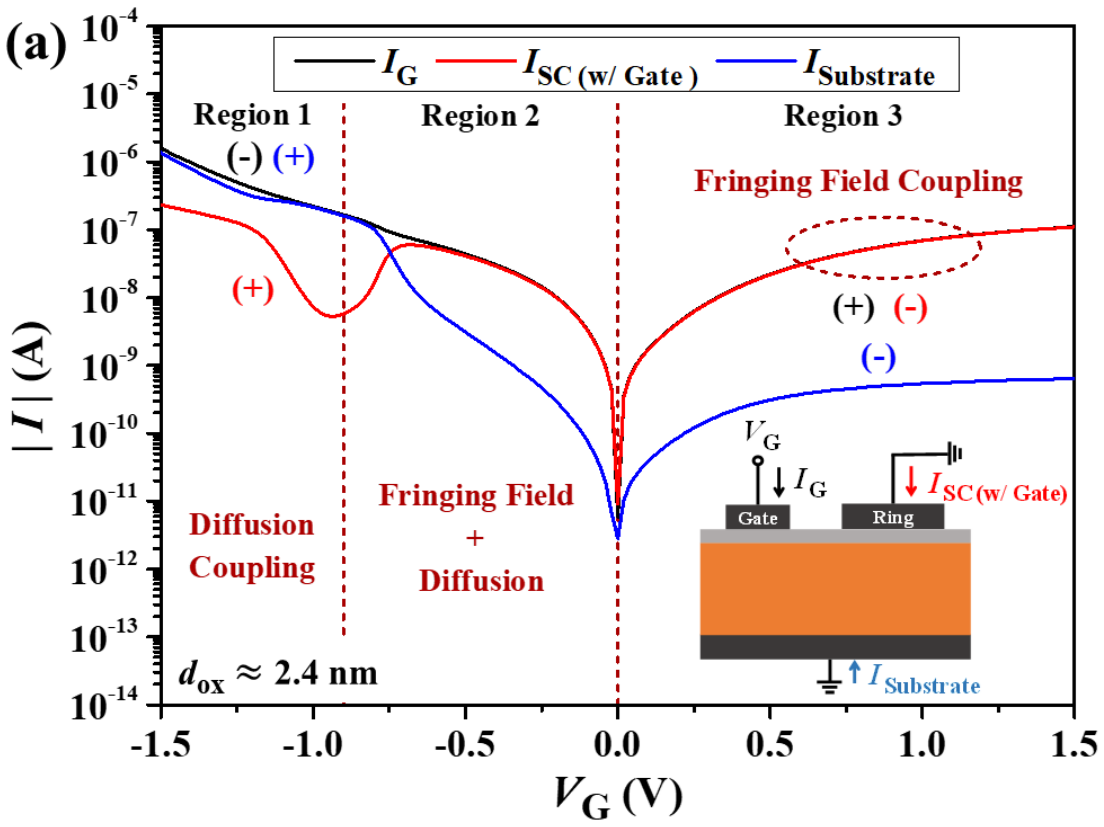

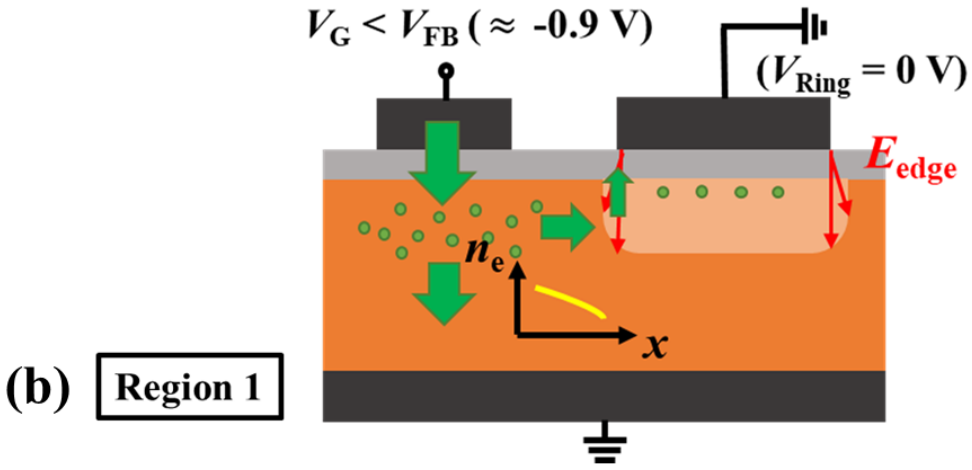

(to be continued)

doi: 10.6342/NTU20230077

`

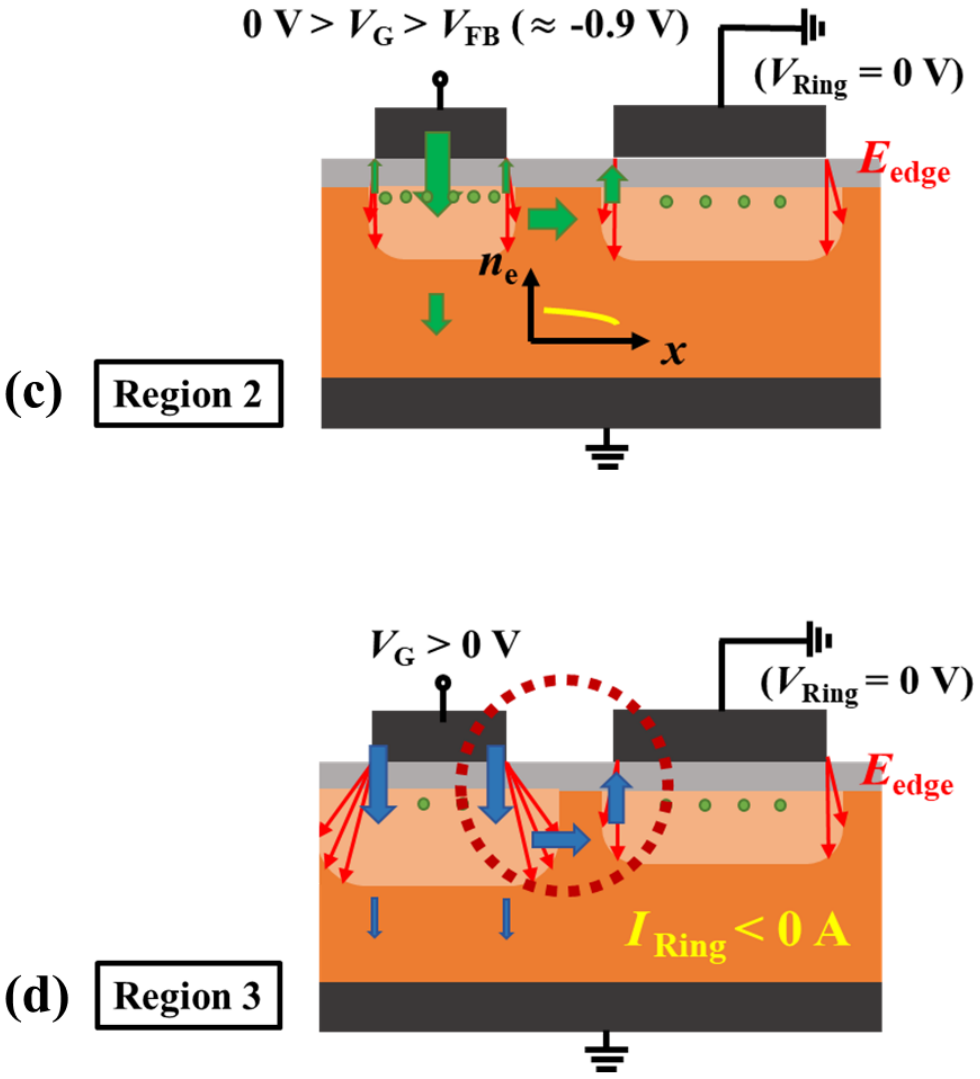

Fig. 2-3. (a) The current at three terminals of the CP-OX concentric device versus the inner gate voltage. The directions of the current flow are marked (+)(-) by the corresponding color. The inset defines the current directions at the three terminals. Schematic diagrams of the coupling mechanism of concentric device under (b) Region 1: $V_G < V_{FB}$, (c) Region 2: 0 V > V_G > V_{FB}, and (d) Region 3: V_G > 0 V. The depletion regions are depicted in light orange, fringing fields are represented by red arrows, and electrons are depicted in green circles. The green and blue arrows represent the electron and hole currents, respectively.

doi: 10.6342/NTU20230077

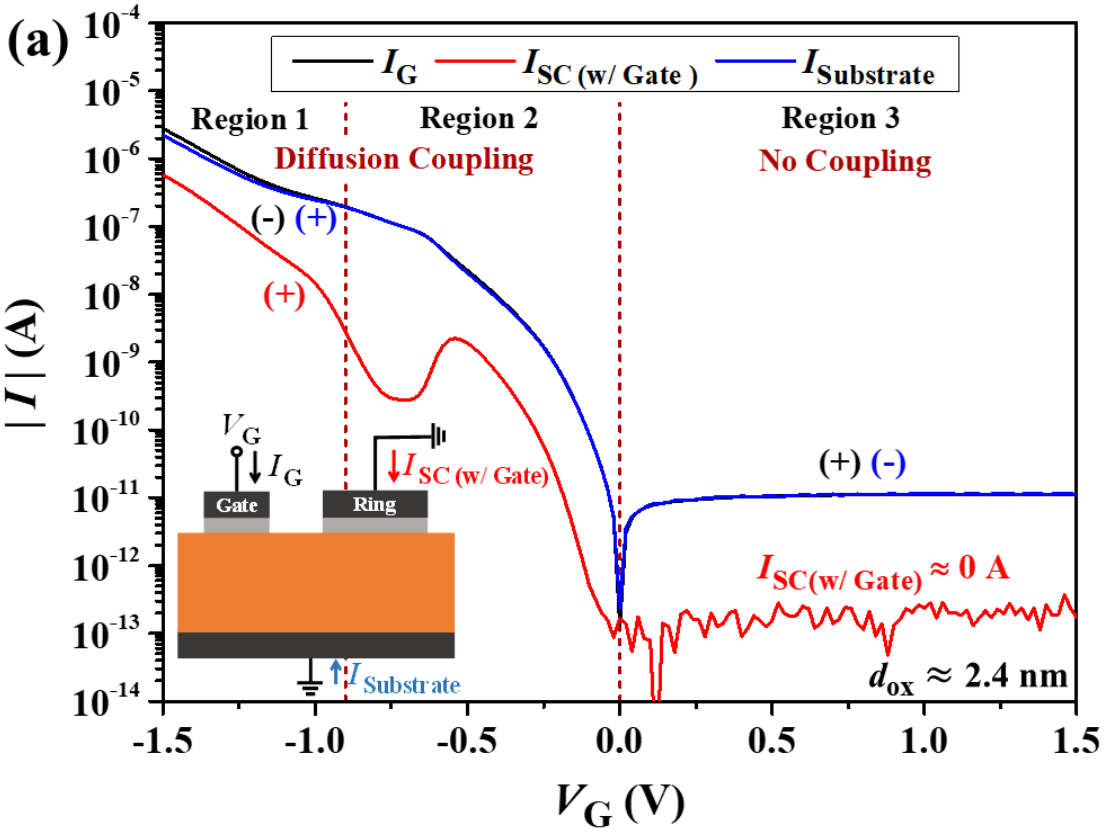

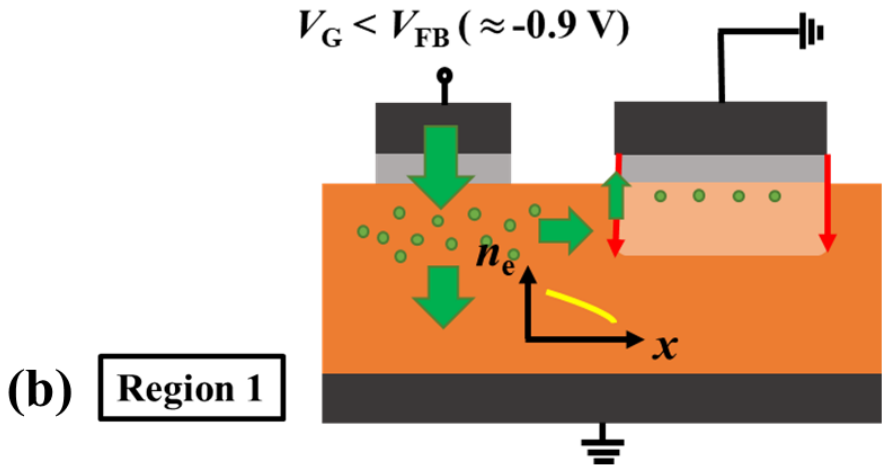

(to be continued)

doi: 10.6342/NTU20230077

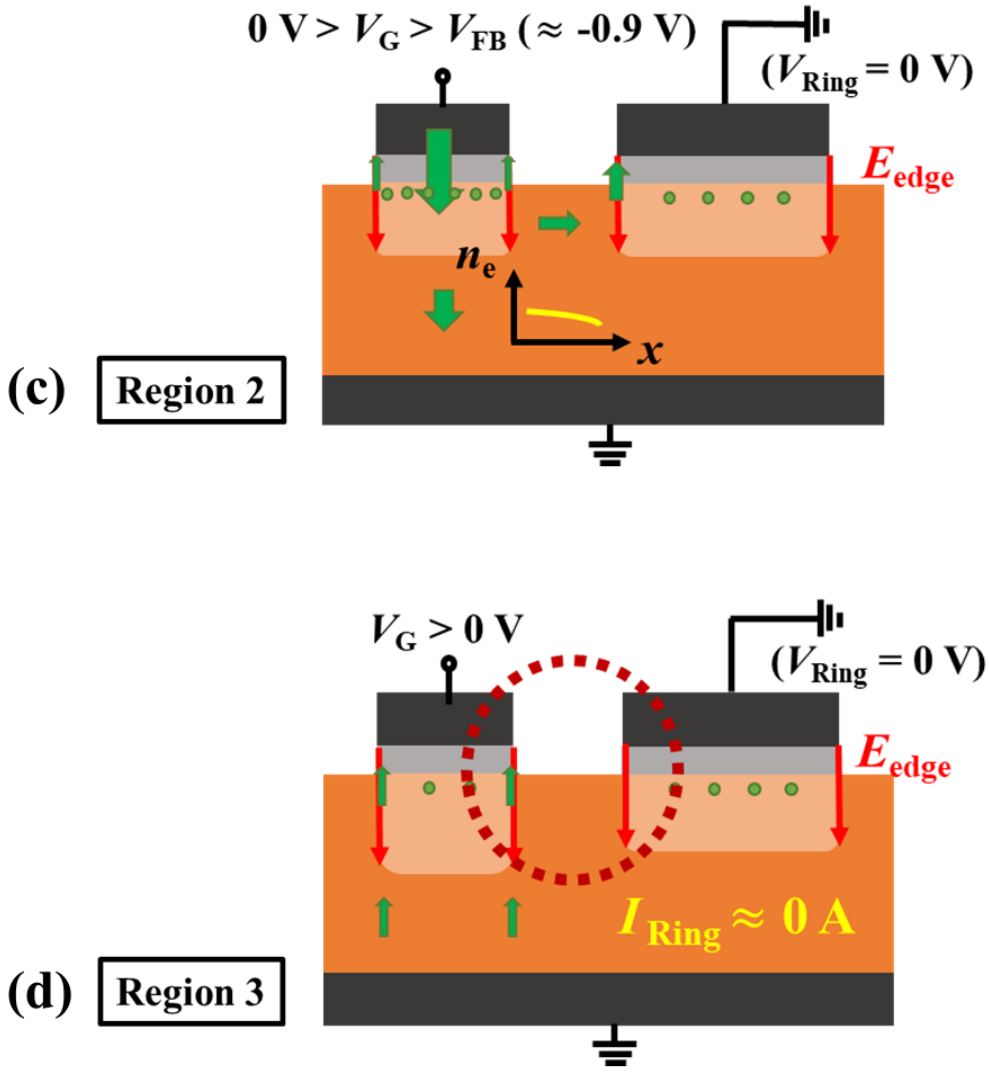

Fig. 2-4. (a) The current at three terminals of the ER-OX concentric device versus the inner gate voltage. The directions of the current flow are marked (+)(-) by the corresponding color. The inset defines the current directions at the three terminals. Schematic diagrams of the coupling mechanism of concentric device under (b) Region 1: $V_G < V_{FB}$, (c) Region 2: 0 V > V_G > V_{FB}, and (d) Region 3: V_G > 0 V. The depletion regions are depicted in light orange, fringing fields are represented by red arrows, and electrons are depicted in green circles. The green and blue arrows represent the electron and hole currents, respectively.

doi: 10.6342/NTU20230077

、

doi: 10.6342/NTU20230077

`

Chapter 3
Photo Sensing in Concentric Devices

3-1 Introduction

3-2 Short-Circuit Operation of Co-Planar Oxide Devices

3-2-1 Current Polarity Changeable

3-2-2 Linear Photodetectivity

3-2-3 Power Consumption

3-3 Short-Circuit Operation of Edge-Removed Oxide Devices

3-3-1 Negligible Dark Current

3-3-2 Substrate Current Depending on Device Size

3-4 Substrate Floating Operation

3-5 Summary

doi: 10.6342/NTU20230077

`

3-1 Introduction

In the previous chapter, we analyzed two categories of concentric MIS(p) TD by short-circuit current and observed that under positive inner gate bias, the short-circuit current of the CP-OX outer ring device is negative, while that of the ER-OX outer ring device is close to zero. This chapter introduced the photo sensing behavior and performance of MIS(p) TDs. We compared two categories of single MIS(p) TDs to concentric MIS(p) TDs that operate with inner gate bias and outer ring short-circuit, exploring their respective advantages and phenomena. Finally, in addition to the short-circuit operation, we also introduced a special operation of the floating substrate and its characteristics.

In this work, we used a white light-emitting diode as the light source for ambient light sensing. The light intensity was measured by TA8131 digital light meter.

3-2 Short-Circuit Operation of Co-Planar Oxide Devices

In this section, all mentioned devices are MIS(p) TDs with CP-OX and an oxide thickness (d_{ox}) of approximately 2.4 nm.

3-2-1 Current Polarity Changeable

Fig. 3-1(a) shows the short-circuit current curves of the outer ring while sweeping the inner gate bias from -1.5 V to 1.5 V under varying light intensities. Due to the photovoltaic effect, an additional photocurrent is generated, resulting in an increase in the short-

doi: 10.6342/NTU20230077

`

circuit current of the outer ring from negative to positive with increasing light intensity under the positive inner gate bias. To describe this phenomenon more clearly, the short-circuit current of the outer ring was measured when it switched between light and dark per second, and the resulting data were plotted in Figs. 3-1(b) and (c). Fig. 3-1(b) shows the case of V_G = 0 V, where I_{SC} increases from near zero, similar to the single device. Fig. 3-1(c) shows the case of V_G = 0.4 V, where I_{SC} can increase from negative to positive. This is a great advantage for photodetection. Different inner gate biases can detect different degrees of light intensity switching from negative to positive.

Fig. 3-2(a) shows the I_{SC} sensing results obtained from different inner gate biases. The light intensity threshold (Φ_{th}) of the current polarity changes at different gate biases is shown in Fig. 3-2(b). The threshold for each gate bias is predicted from the linear relationship in Fig. 3-2(a). Take V_G = 0.4 V as an example, referring to Fig. 3-2(a), a negative current is detected in the dark, whereas a positive current is observed at a light intensity of approximately 140 lux. This allows easy discrimination of light intensities above a specific threshold. Moreover, weak light can also be detected by using a smaller inner gate bias.

3-2-2 Linear Photodetectivity

The relationship between the short-circuit current and light intensity at different inner gate biases is shown in Fig. 3-2(a). The linear relationship appears above 100 lux, and

doi: 10.6342/NTU20230077

`

all the coefficients of determination between the data and the linear fitting curves are greater than 0.998. The slope representing sensitivity in this range indicates good responsivity and linearity. Therefore, our device has good potential for photosensitivity.

Notably, the sensing results of concentric devices at higher gate voltages exhibited significant variation compared to that of single devices under weak light conditions. Fig. 3-3 can further explain this phenomenon, where the outer ring remains at 0 V and a positive inner gate bias is applied. The depletion region in the dark is identified as the light orange region. However, when exposed to light, the generation of electron-hole pairs introduces additional carriers to the depletion region, causing it to shrink [15], which is marked as yellow dashed lines. When the depletion width reduces, the coupling effect weakens because the fringing field also decreases. Therefore, in addition to the photogenerated current of the ring device, the responsivity of the concentric device is enhanced under weak light due to the synergistic effect caused by the weakened coupling of inner gates. However, as the coupling effect decreases with increasing light intensity, the photogenerated current dominates the responsivity. This indicates that the short-circuit current is proportional to the light intensity.

3-2-3 Power Consumption

Due to the short-circuit operation, power (P) is only generated from the inner gate, and can be calculated by multiplying the gate voltage (V_G) by the gate current (I_G):

doi: 10.6342/NTU20230077

`

$$P = V_G \times I_G \quad (3\text{-}1)$$

Fig. 3-4(a) illustrates the I_G-V_G curves with outer ring short-circuit operation under varying light intensities. Due to the coupling effect of the outer ring to the inner gate, the current only shows a small increase under illumination [14]. Hence, utilizing the inner center as a gate can result in lower power consumption. Fig. 3-4(b) shows the power consumption calculated by Eq. (3-1) based on the data extracted from Fig. 3-4(a) at different gate biases. Due to the short-circuit operation, the power consumption is reduced compared to the conventional deep depletion current-sensing method [14]. The power consumption is below 100 nW in this work.

3-3 Short-Circuit Operation of Edge-Removed Oxide Devices

In this section, all mentioned devices are MIS(p) TDs with ER-OX.

3-3-1 Negligible Dark Current

In this subsection, the oxide layer thickness (d_{ox}) of the devices is approximately 2.4 nm. Fig. 3-5 shows the short-circuit current curves of the outer ring while sweeping the inner gate bias from -1.5 V to 1.5 V under varying light intensities. As the positive inner gate bias continues to increase, the short-circuit current of the outer ring remains almost constant due to the absence of a coupling effect in this region, as described in Section 2-3-3. This indicates that the current behavior is similar to that of a single device regardless

doi: 10.6342/NTU20230077

`

of the inner gate bias. Fig. 3-6 shows the short-circuit current of the concentric outer ring under different inner gate biases, as well as a comparison to the single ring device.

3-3-2 Substrate Current Depending on Device Size

Although the short-circuit current of the outer ring with inner gate bias of the concentric device behaves similarly to that of the single device, we observed an interesting phenomenon due to the negligible dark current of the outer ring short-circuit operation. The devices mentioned in this subsection have an oxide layer thickness (d_{ox}) of approximately 2.3 nm. Fig. 3-7(a) shows that in the dark condition, the current measured in the substrate of the concentric device is mainly attributed to the inner gate current because the outer ring is at zero bias and no current will flow to the substrate at this time. Fig. 3-7(b) shows that in the presence of light, both the inner gate and the outer ring have additional photocurrent flowing to the substrate due to the photovoltaic effect, and the current measured is primarily influenced by the outer ring. This phenomenon shows that a concentric device has a better light-to-dark current ratio than a positively biased single device. In single devices, the photocurrent and dark current are positively correlated with their size, meaning that while larger sizes generate higher photocurrent, they also produce higher dark current. By utilizing the concentric device, where the outer ring and substrate are both biased at 0 V, we can obtain higher photocurrent and lower dark current by measuring the substrate current.

doi: 10.6342/NTU20230077

`

To express this device size-dependent phenomenon more clearly, Fig. 3-8 and Fig. 3-9 demonstrate the substrate current versus inner gate voltage curves for concentric devices of different sizes. Fig. 3-8(a) shows the $I_{substrate}$-V_G curves for four different inner gate radii, with the outer radius of the outer ring fixed at 600 μm. It is observed that the photocurrents of the four curves in the positive bias region almost overlap, indicating that the outer perimeter of the outer ring dominates the photocurrent of the concentric device. Moreover, we divided the current shown in Fig. 3-8(a) by the respective perimeter of the inner gate and the results are shown in Fig. 3-8(b). It is found that the dark currents of the four curves in the positive bias region coincide, indicating that the perimeter of the inner gate dominates the dark current of the concentric device. In addition, Fig. 3-9(a) also shows the $I_{substrate}$-V_G curves for three different outer ring radii with the inner gate radius fixed at 85 μm. It is found that the dark currents of the four curves in the positive bias region coincide. Similarly, the current shown in Fig. 3-9(a) was divided by the respective outer perimeter of the outer ring and the results are shown in Fig. 3-9(b). It is observed that the photocurrents of the three curves in the positive bias region almost overlap. These results are consistent with Fig. 3-8.

3-4 Substrate Floating Operation

This section introduces a special operation mode of concentric devices with an oxide layer thickness (d_{ox}) of approximately 2.3 nm. In this mode, the substrate is floating, the

doi: 10.6342/NTU20230077

`

inner center is grounded, and the outer ring is swept from -1.5 V to 1.5 V. This method produced an interesting phenomenon that was observed in the CP-OX and ER-OX structures, as shown in Fig. 3-10(a) and Fig. 3-12(a), respectively. The current exhibited a saturated low value in both the negative and positive voltage regions.

In order to explain this phenomenon, we compared them to the general measurement method, in which the *I-V* curves are measured with the grounded substrate. Fig. 3-10(b) and Fig. 3-12(b) show the outer ring current curves of CP-OX and ER-OX, respectively, with both the inner center and substrate grounded, and the outer ring voltage swept from -1.5 V to 1.5 V under varying light intensities. Fig. 3-10(c) and Fig. 3-12(c) show the inner center current curves of CP-OX and ER-OX, respectively, with both the outer ring and substrate grounded, and the inner center voltage swept from -1.5 V to 1.5 V under varying light intensities.

It is worth noting that the outer ring current value under positive outer ring voltage in the case of the floating substrate is similar to that in the case of the grounded substrate, as shown in Fig. 3-11(a) for CP-OX and Fig. 3-13(a) for ER-OX. However, the outer ring current value under negative outer ring voltage in the case of the floating substrate is similar to the inner center current value in the case of the grounded substrate, grounded outer ring, and positively biased inner center, as shown in Fig. 3-11(b) for CP-OX and Fig. 3-13(b) for ER-OX. The reasons for this phenomenon will be explained in the

doi: 10.6342/NTU20230077

`

following paragraphs.

When the substrate is floating, no current flows through it. However, by applying a bias voltage to one MIS(p) TD while grounding the neighboring one, the floating substrate can detect an induced voltage signal, preventing any leakage current from passing through it. Fig. 3-14 shows the induced voltage of the floating substrate of CP-OX and ER-OX under varying light intensities in the outer ring voltage range of -1.5 V to 1.5 V. The results show that the substrate-induced voltage closely matches the outer ring voltage when the outer ring voltage is negative. However, with a positive outer ring voltage, the substrate-induced voltage only slightly increases. This is because a positive outer ring bias voltage robs electrons in the substrate, inducing a positive voltage and making the inner center a negative potential relative to the substrate. For MIS(p) TD at negative bias, a small negative voltage is sufficient to generate a current that corresponds to the saturated current under positive bias, thereby achieving equilibrium. Similarly, when the outer ring is negatively biased, the substrate obtains electrons, inducing a negative voltage and making the inner center a positive potential relative to the substrate. To achieve a consistent amount of current flow between the outer ring and the inner center, only a small negative voltage difference between the outer ring and the substrate is needed to generate the same amount of saturation current as a positive voltage difference between the inner center and the substrate.

doi: 10.6342/NTU20230077

`

When the light is illuminated, an additional current is generated due to the photovoltaic effect, so the induced voltage of the substrate changes as shown in Fig. 3-14, and the *I-V* curve will not shift to the left like the case where the substrate is grounded. Therefore, by this operation, it can be used to detect the light intensity in both positive bias and negative bias. Moreover, compared with CP-OX and ER-OX, the light-to-dark current ratio of ER-OX is better because it has a lower dark current and no coupling effect.

3-5 Summary

In the beginning of this chapter, we present the advantages of two categories of concentric MIS(p) TDs in light sensing with inner gate bias and outer ring short-circuit operation. Different categories of MIS(p) TDs exhibit different phenomena and applications.

For the case of MIS(p) TDs with CP-OX, the coupling effect of different gate biases can help to easily distinguish light intensities above a specific threshold, which means different degrees of light intensity switching from negative to positive can be detected by adjusting the gate bias voltage, while the linear photodetectivity can ensure reliable measurement of light signals. Moreover, this approach also leads to low power consumption.

For the case of MIS(p) TDs with ER-OX, the substrate current detection shows that the dark current is proportional to the perimeter of the inner gate, while the photocurrent is proportional to the outer perimeter of the outer ring. As a result, a better light-to-dark current ratio can be obtained by adjusting the size of the inner gate and the outer ring.

doi: 10.6342/NTU20230077

`

At the end of this chapter, we introduce the light-sensing advantages of concentric MIS(p) TDs under floating substrate operation. In this way, photodetection can be operated under negative bias as well as positive bias.

doi: 10.6342/NTU20230077

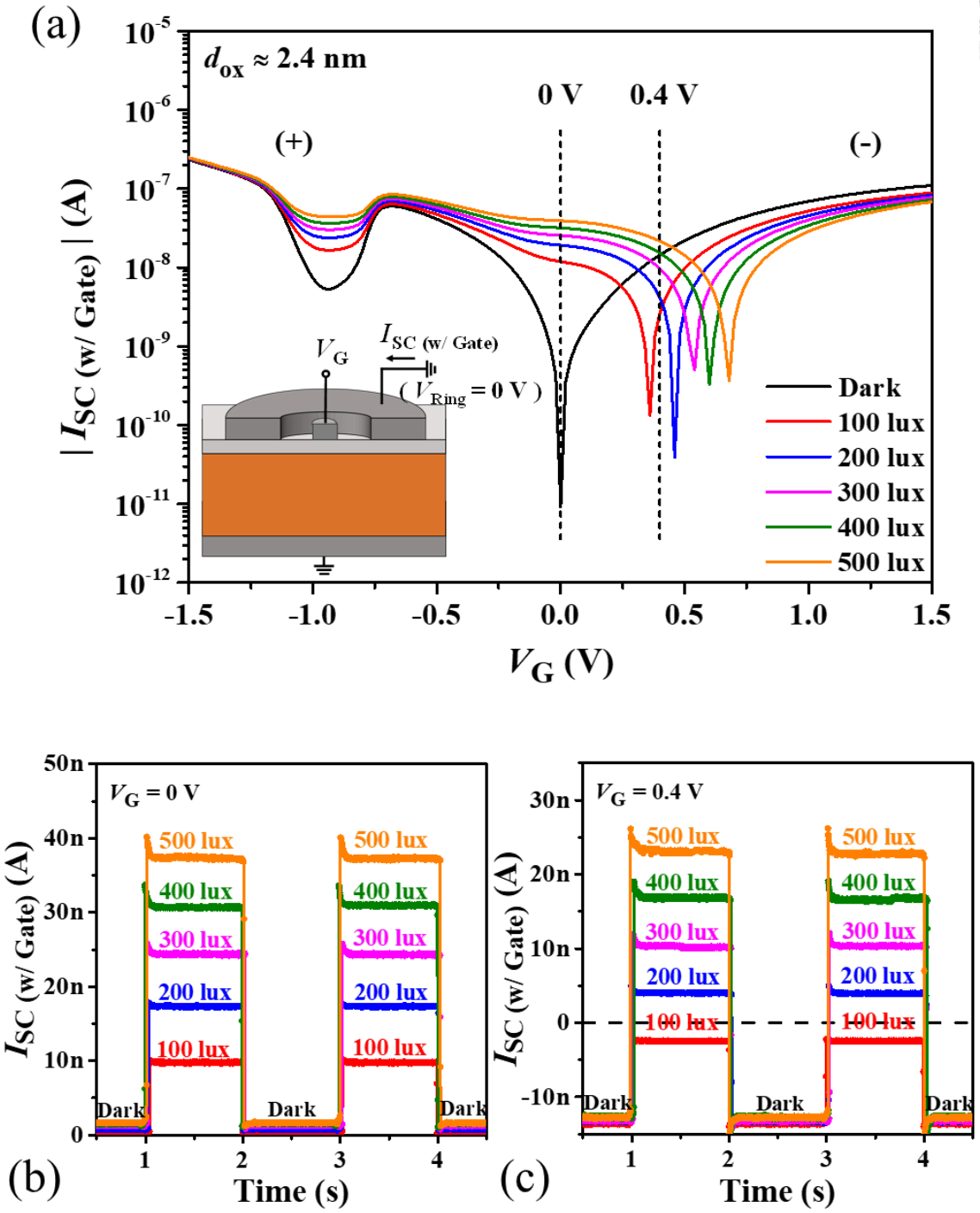

Fig. 3-1. (a) The short-circuit current of the CP-OX outer ring versus the inner gate voltage and the *I-t* diagrams switching between light and dark conditions per second at (b) V_G = 0 V and (c) V_G = 0.4 V under varying light intensities.

doi: 10.6342/NTU20230077

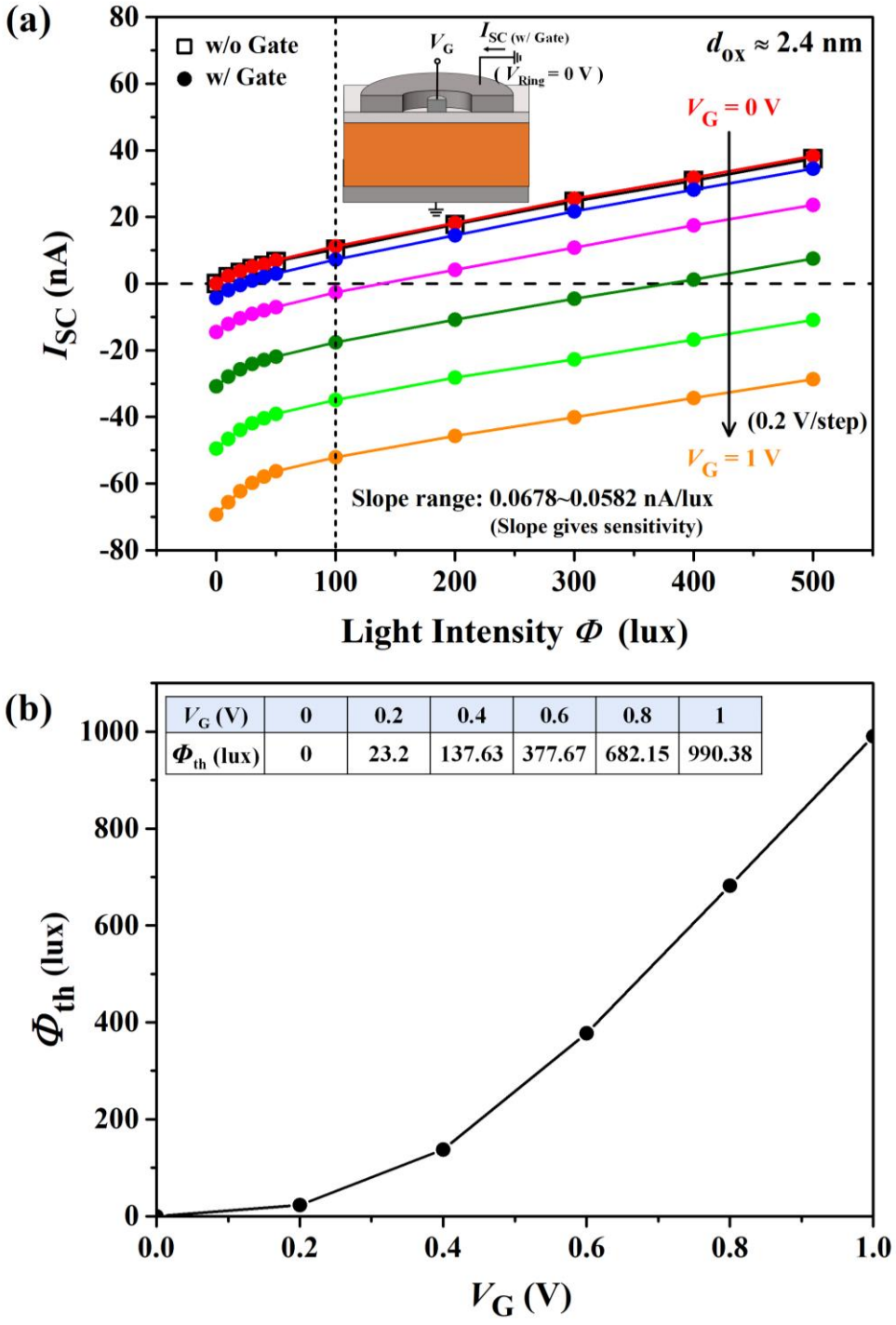

Fig. 3-2. (a) The short-circuit current (I_{SC}) of different inner gate biases (V_G) under varying light intensities (Φ). The linear range occurs when the light intensity is greater than 100 lux. The slope of the fitted curve is also indicated. (b) Light intensity threshold (Φ_{th}) for current polarity changes under different inner gate biases (V_G). The thresholds for each bias were predicted from linear relationships.

doi: 10.6342/NTU20230077

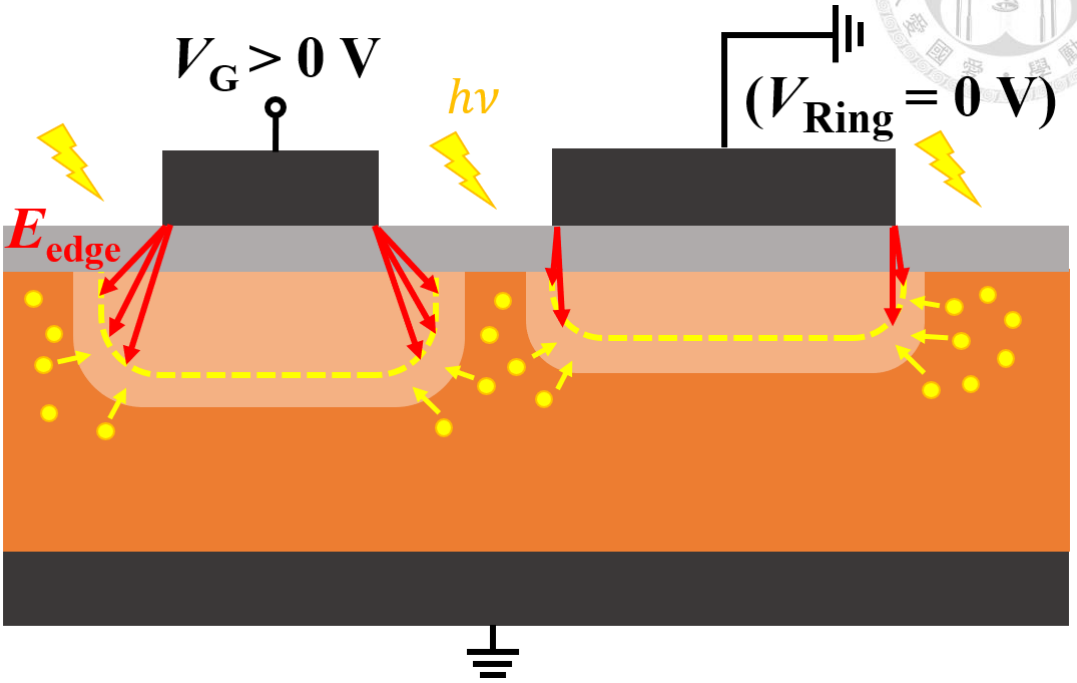

Fig. 3-3. Schematic diagram of the fringing field under illumination. The fringing fields are indicated by red arrows. The yellow circles represent the additional photogenerated electrons. The light orange area indicates the depletion region in the dark, while the dashed yellow line indicates the depletion region boundary that contracts inward under illumination.

doi: 10.6342/NTU20230077

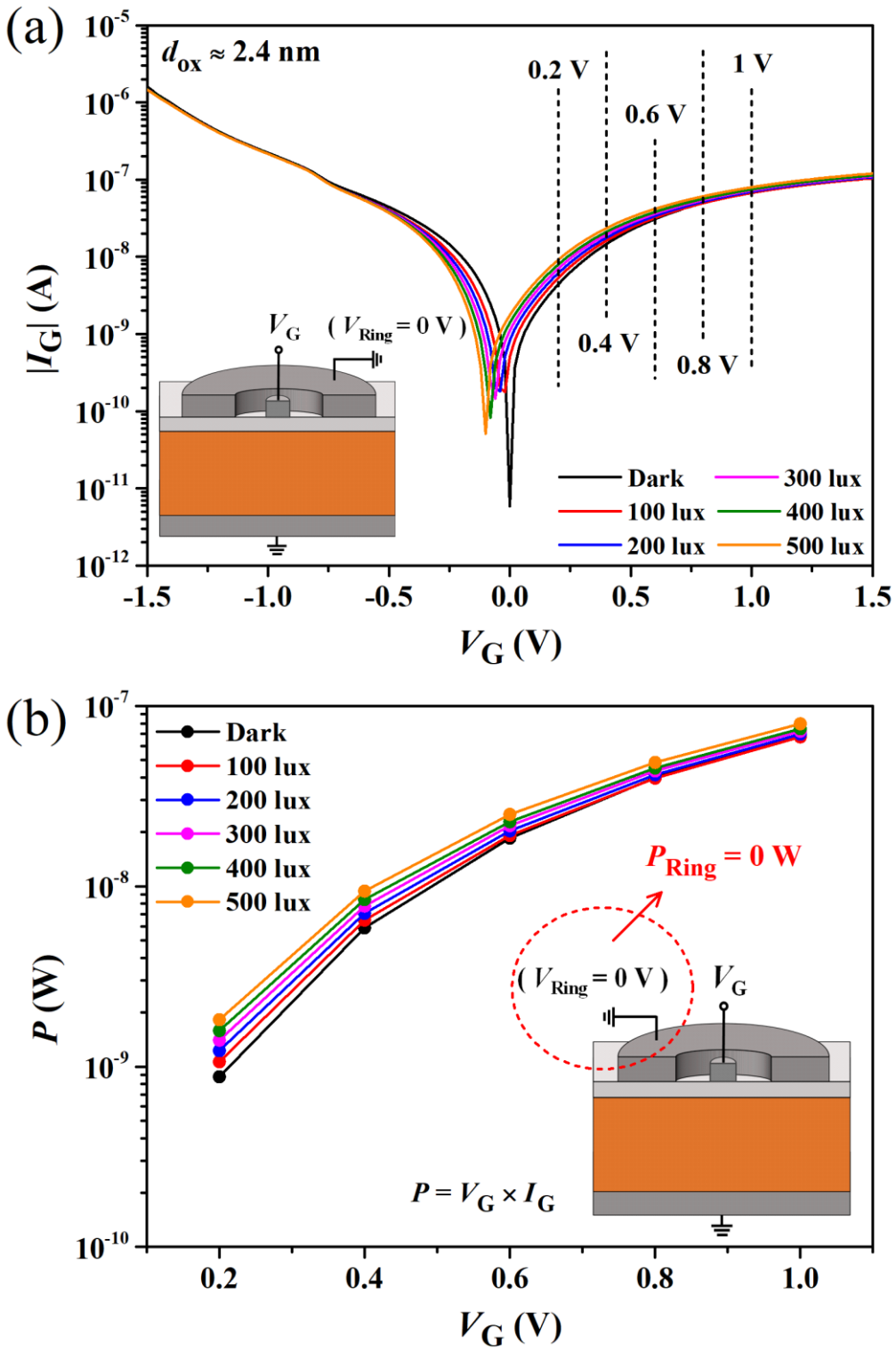

Fig. 3-4. (a) I_G-V_G curves with the CP-OX outer ring biased at 0 V under varying light intensities. (b) Power consumption at different gate biases obtained from (a).

doi: 10.6342/NTU20230077

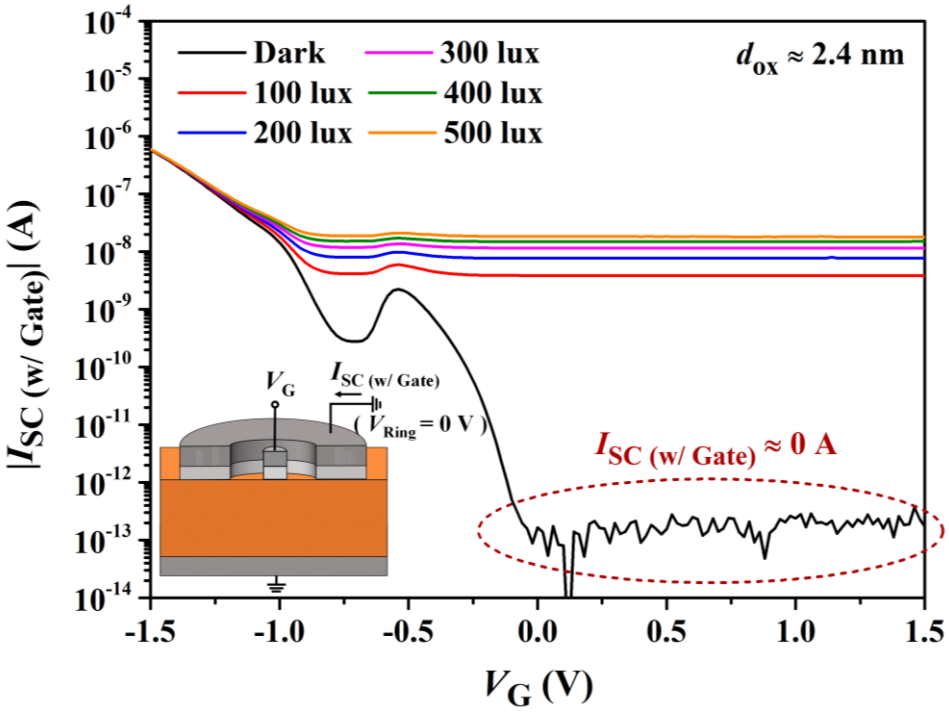

Fig. 3-5. (a) The short-circuit current of the ER-OX outer ring versus the inner gate voltage under varying light intensities. Due to the absence of coupling effects, the short-circuit current at positive bias is similar to that of a single device.

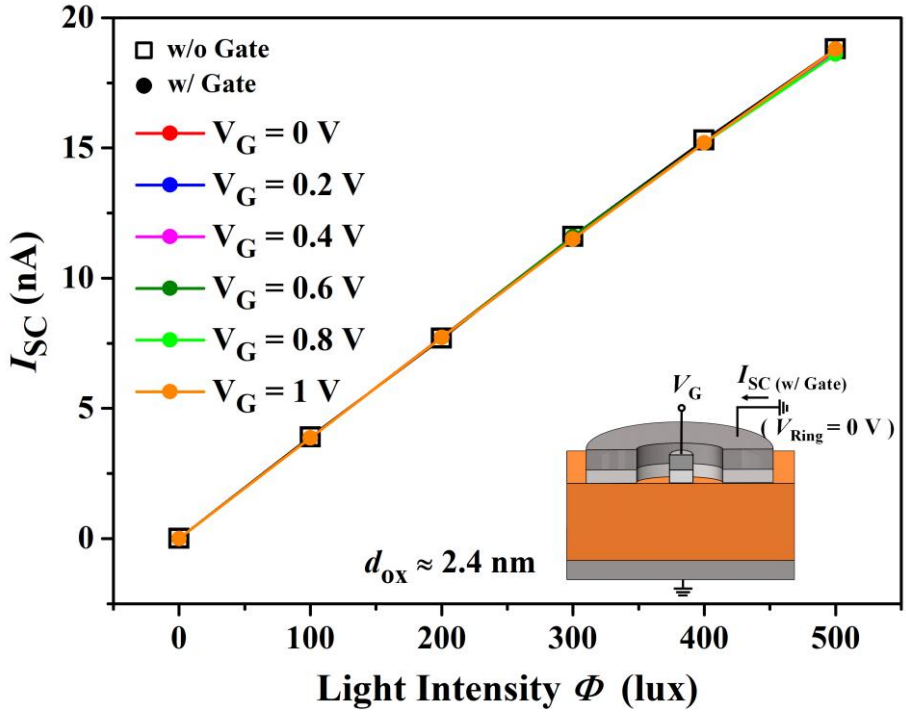

Fig. 3-6. The short-circuit current (I_{SC}) of the ER-OX outer ring under different inner gate biases (V_G) versus varying light intensities (Φ). The concentric device senses the same short-circuit current as a single device regardless of the inner gate positive bias.

doi: 10.6342/NTU20230077

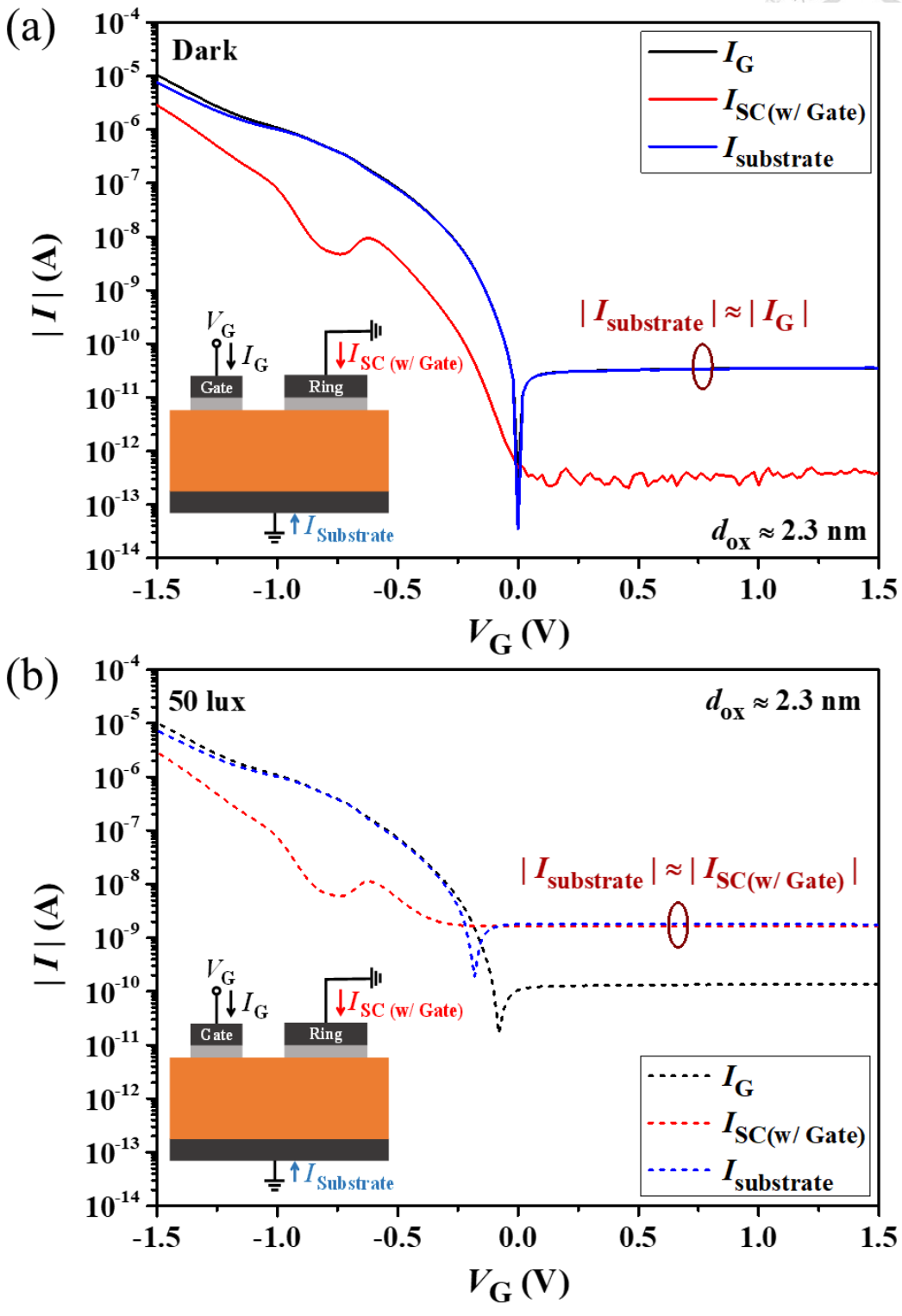

Fig. 3-7. The current at three terminals of the ER-OX concentric device versus the inner gate voltage (a) in the dark and (b) at the light intensity of 50 lux. The substrate current is dominated by the inner gate in the dark and by the outer ring under illumination.

doi: 10.6342/NTU20230077

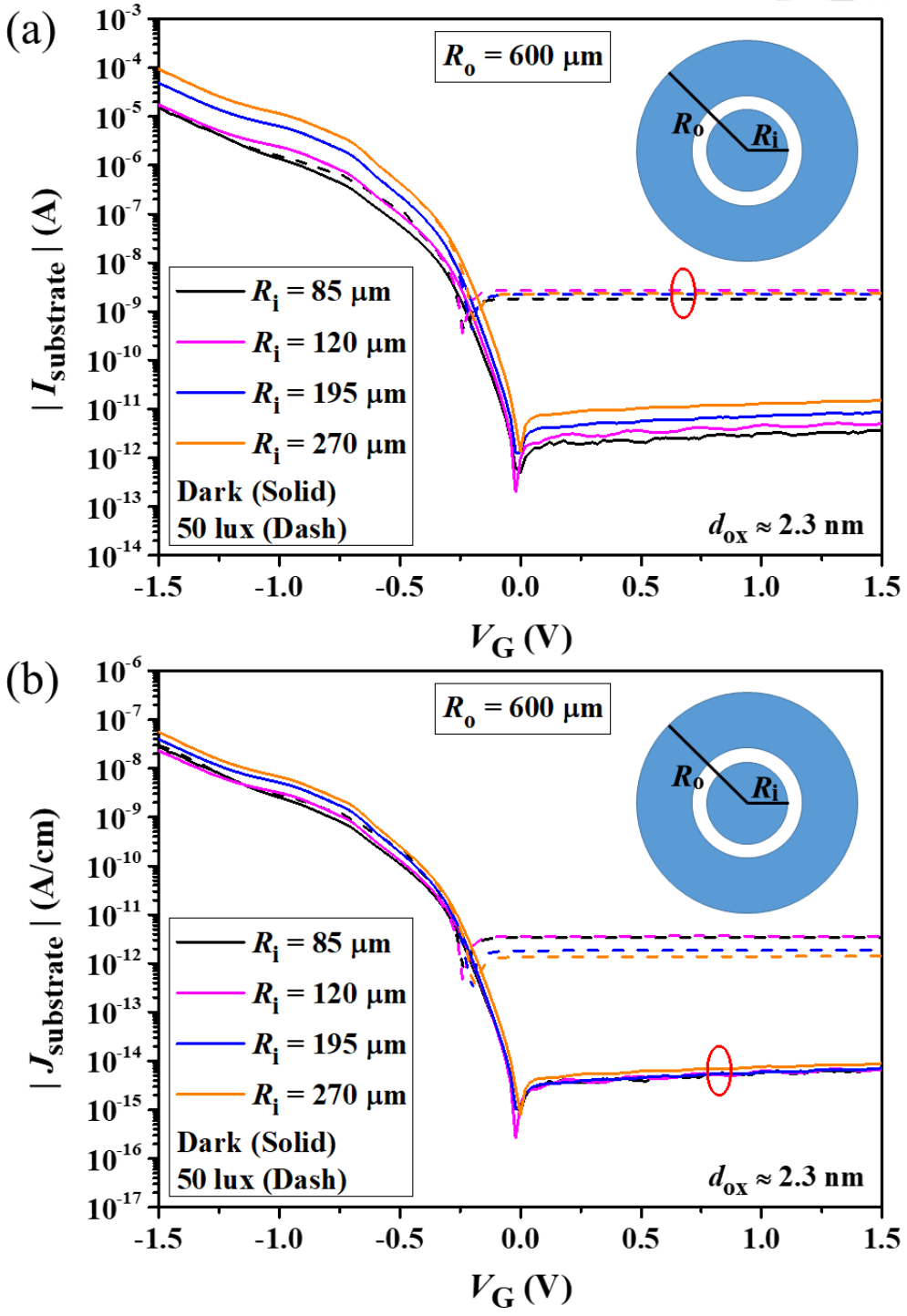

Fig. 3-8. (a) $I_{substrate}$-V_G curves of ER-OX concentric devices with different inner circle radii but the fixed outer radius of the outer ring under dark and illuminated conditions. The photocurrents of the four curves in the positive bias region almost overlap. (b) Substrate current shown in (a) divided by the perimeter of the corresponding inner gate versus inner gate voltage. The dark currents of the four curves in the positive bias region coincide.

doi: 10.6342/NTU20230077

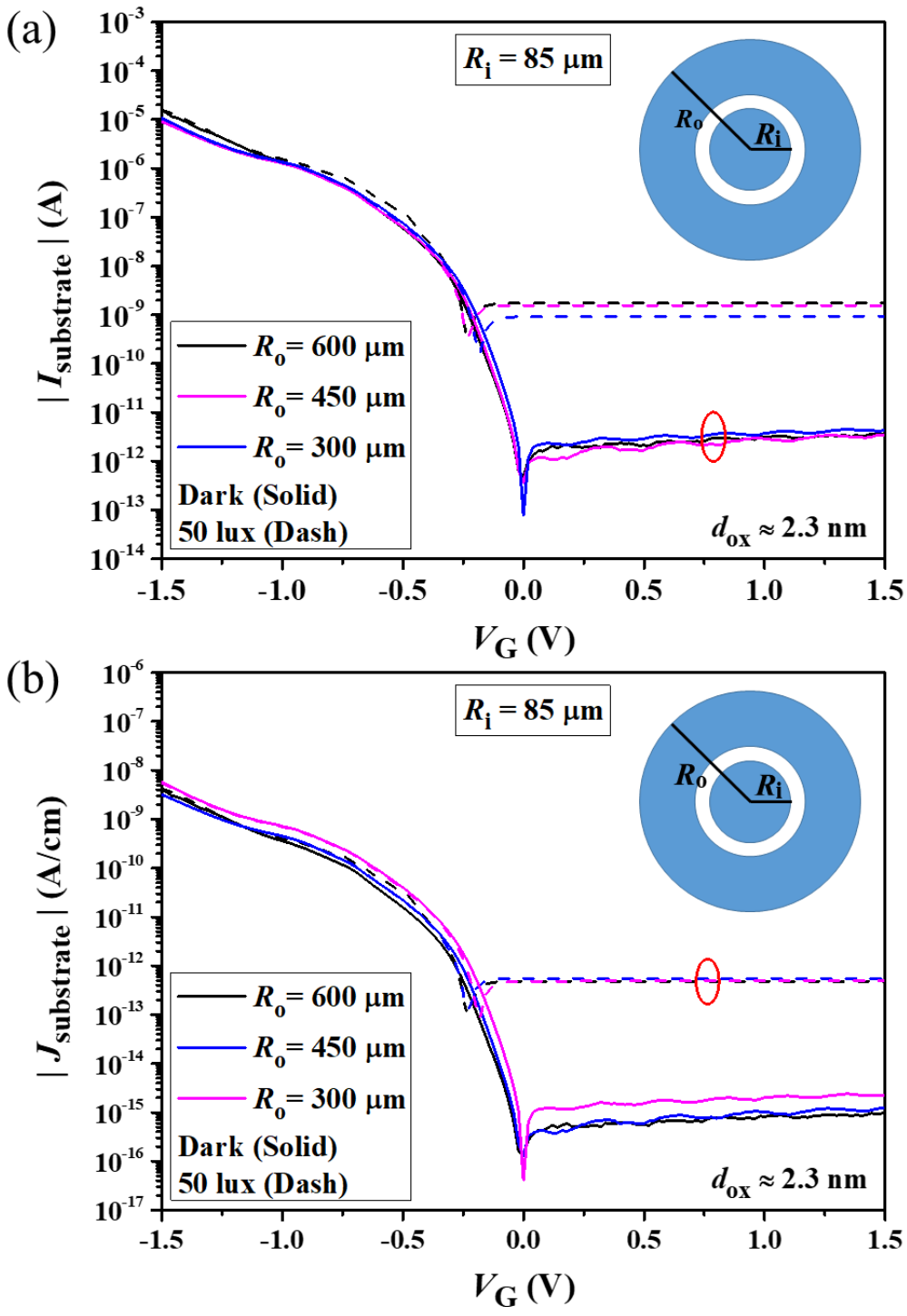

Fig. 3-9. (a) $I_{substrate}$-V_G curves of ER-OX concentric devices with different outer radii of the outer ring but fixed inner circle radius under dark and illuminated conditions. The dark currents of the three curves in the positive bias region coincide. (b) Substrate current shown in (a) divided by the outer perimeter of the corresponding outer ring versus the inner gate voltage. The photocurrents of the three curves in the positive bias region almost overlap.

doi: 10.6342/NTU20230077

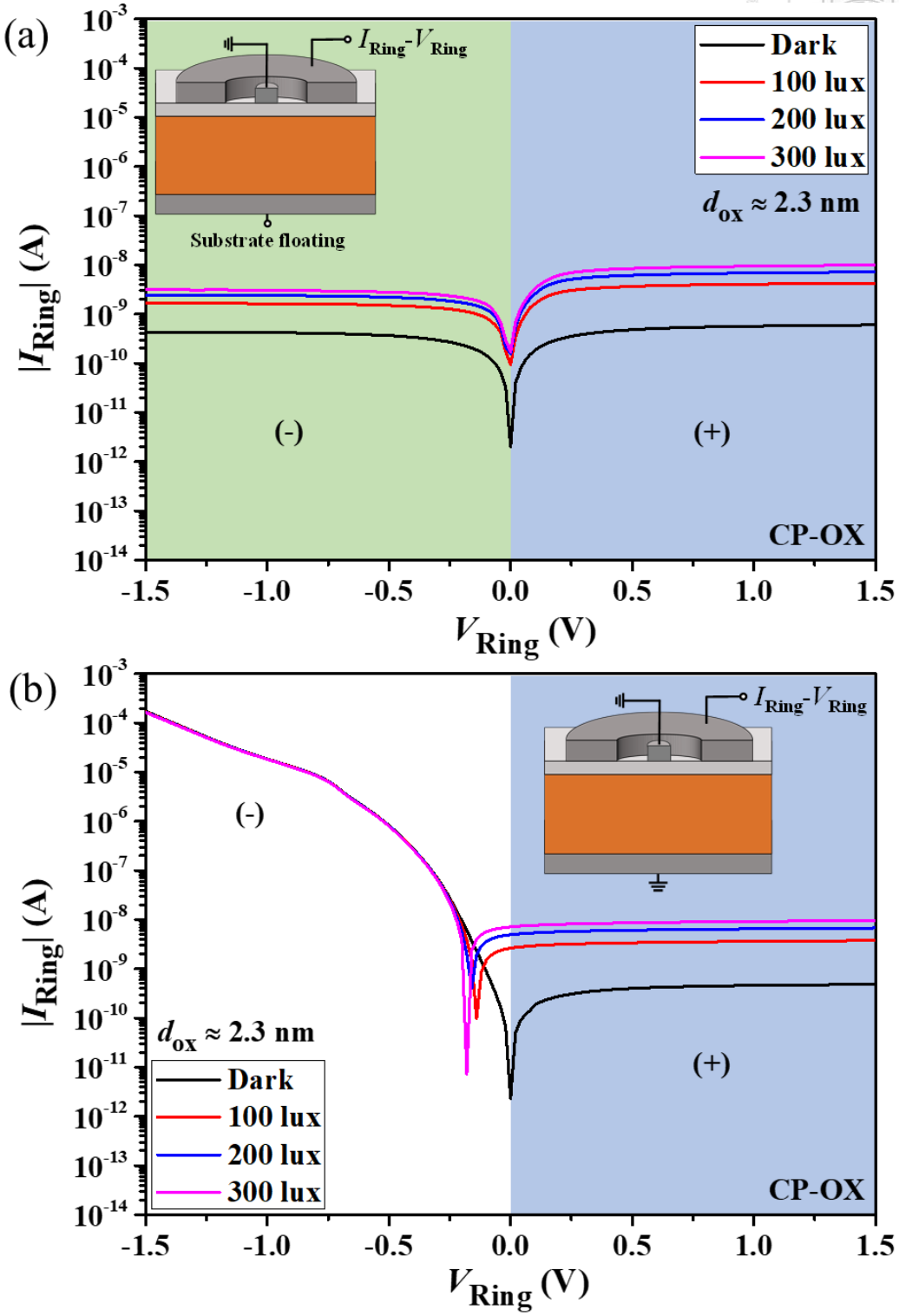

(to be continued)

doi: 10.6342/NTU20230077

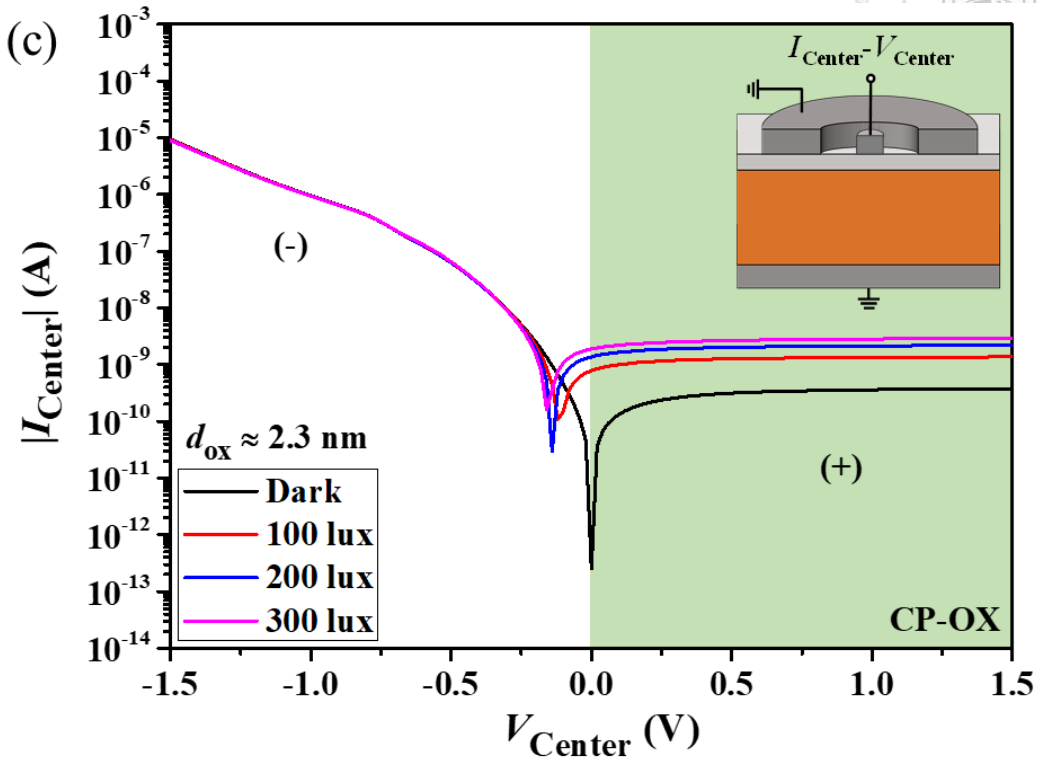

Fig. 3-10. (a) I_{Ring}-V_{Ring} curves of substrate floating and inner center grounded, (b) I_{Ring}-V_{Ring} curves of substrate and inner center both grounded, and (c) I_{Center}-V_{Center} curves of substrate and outer ring both grounded under varying light intensities for CP-OX. The saturation current value in the positive voltage region of graph (a) is consistent with that of graph (b), while the saturation current value in the negative voltage region of graph (a) is consistent with that in the positive voltage region of graph (c).

doi: 10.6342/NTU20230077

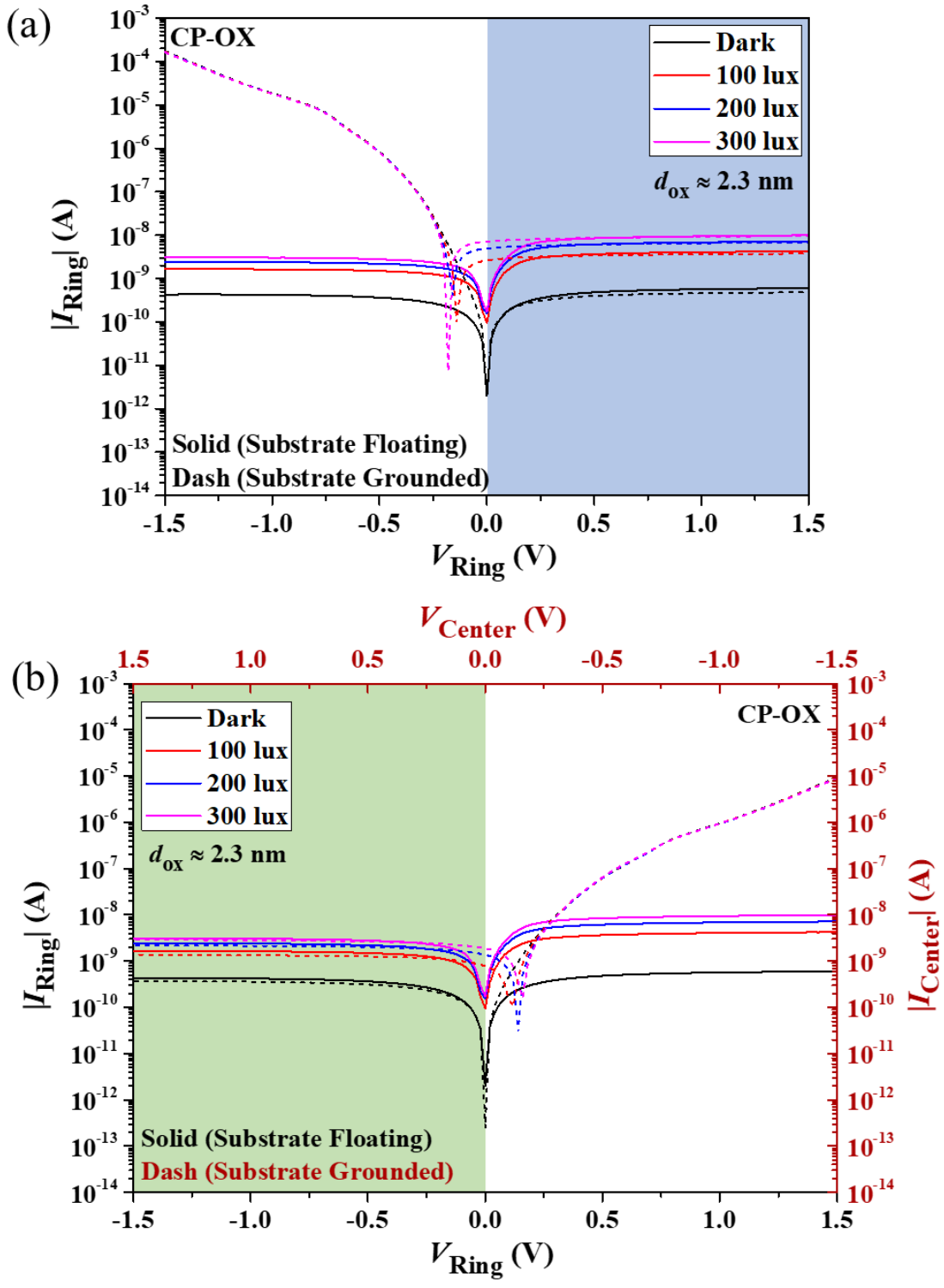

Fig. 3-11. (a) Overlay of Figs. 3-10(a) and (b). (b) Overlay of Figs. 3-10(a) and (c).

doi: 10.6342/NTU20230077

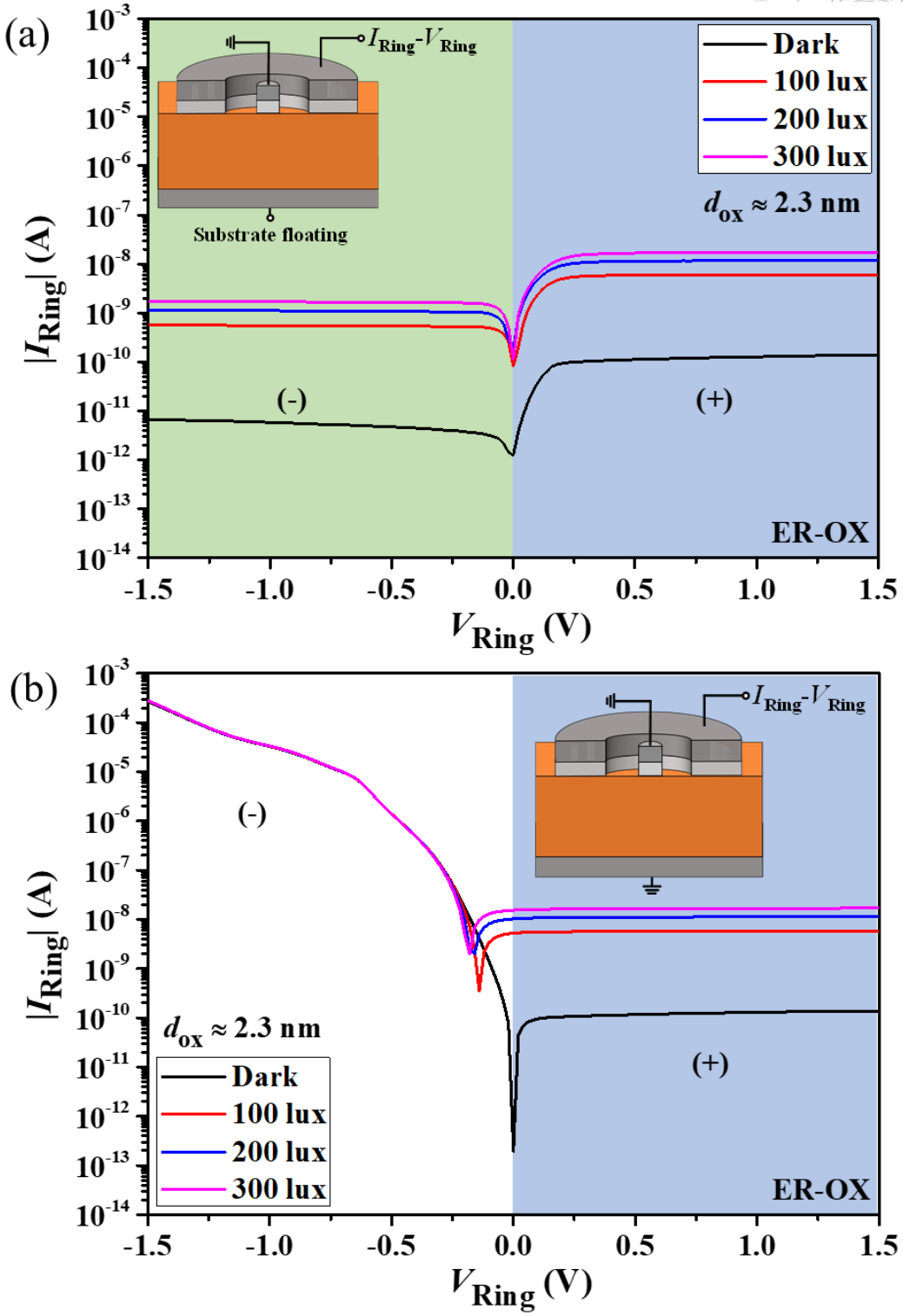

(to be continued)

doi: 10.6342/NTU20230077

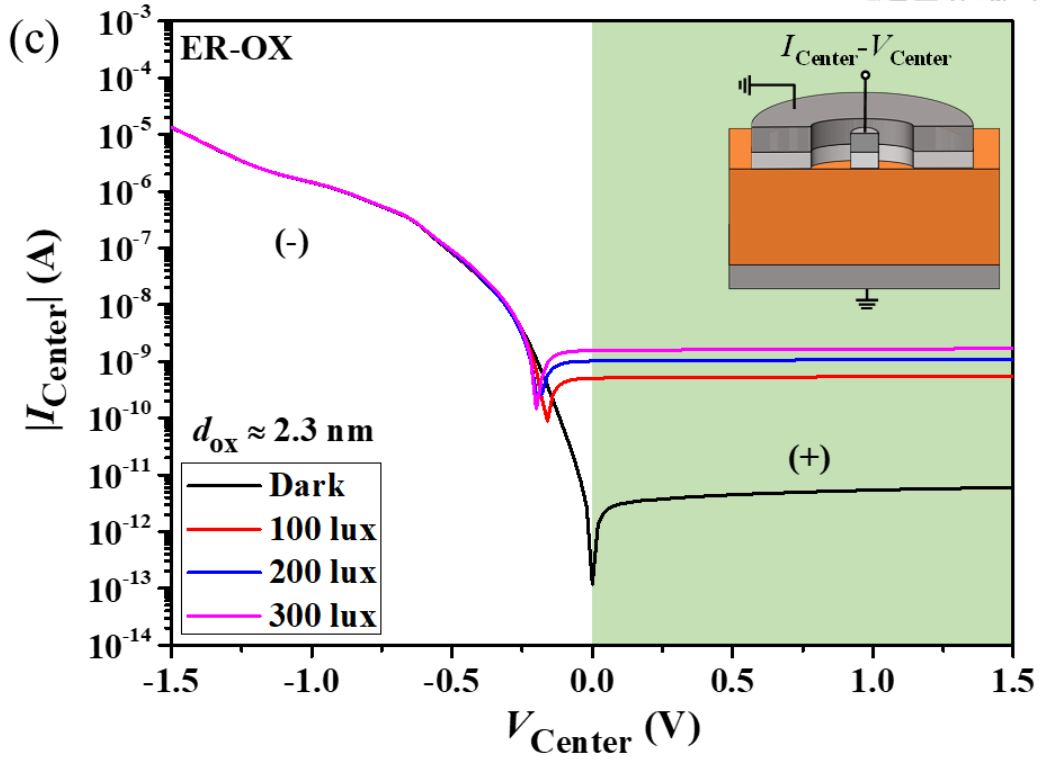

Fig. 3-12. (a) I_{Ring}-V_{Ring} curves of substrate floating and inner center grounded, (b) I_{Ring}-V_{Ring} curves of substrate and inner center both grounded, and (c) I_{Center}-V_{Center} curves of substrate and outer ring both grounded under varying light intensities for ER-OX. The saturation current value in the positive voltage region of graph (a) is consistent with that of graph (b), while the saturation current value in the negative voltage region of graph (a) is consistent with that in the positive voltage region of graph (c).

doi: 10.6342/NTU20230077

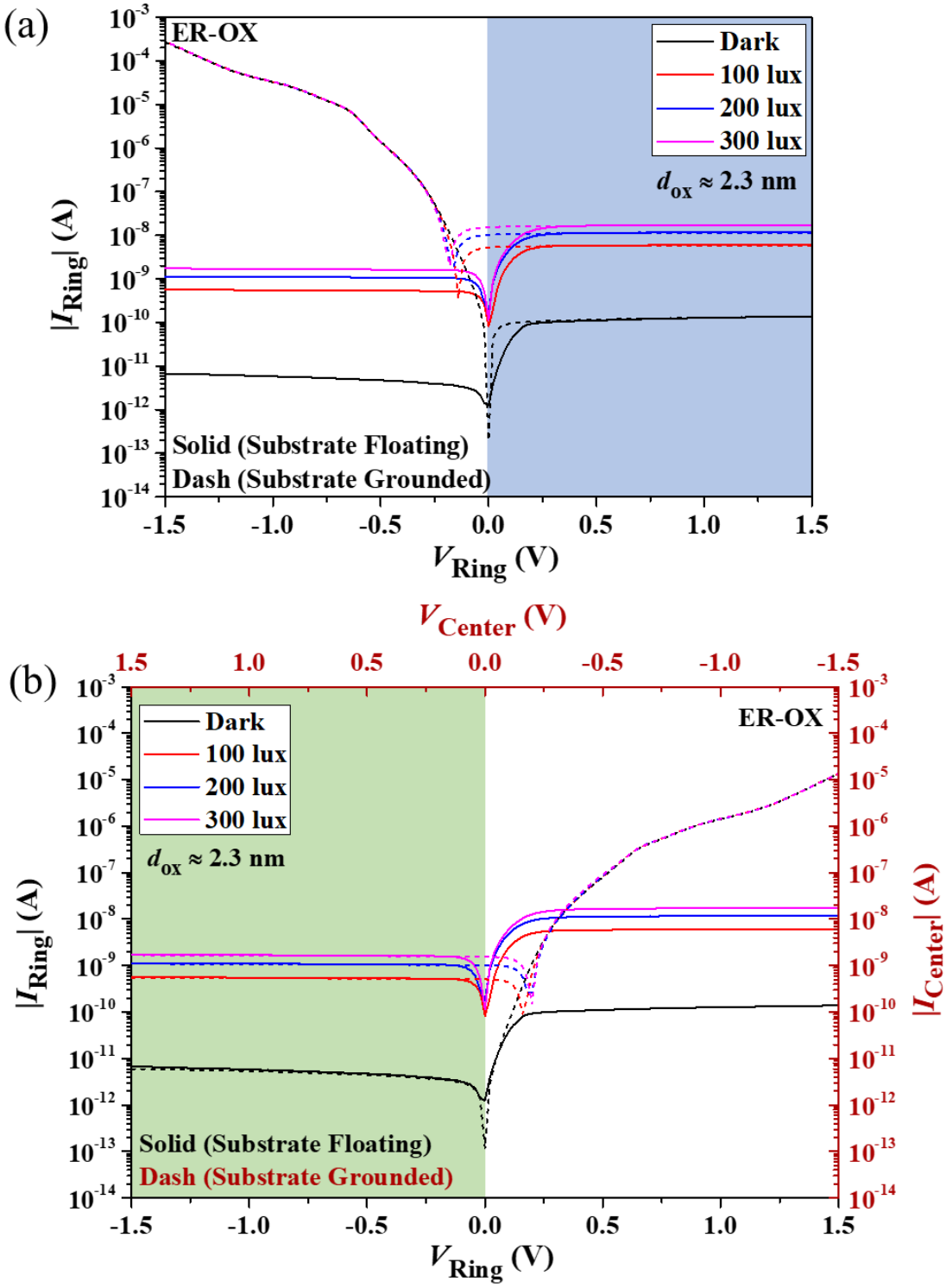

Fig. 3-13. (a) Overlay of Figs. 3-12(a) and (b). (b) Overlay of Figs. 3-12(a) and (c).

doi: 10.6342/NTU20230077

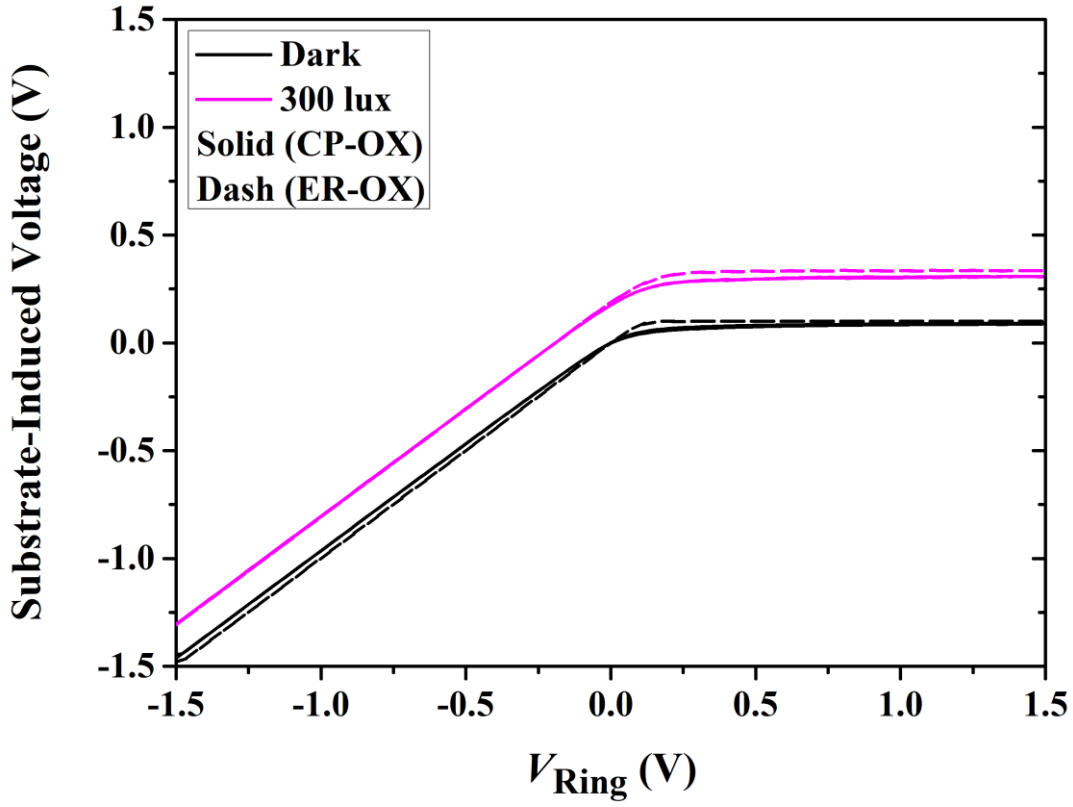

Fig. 3-14. Substrate-induced voltage versus the outer ring voltage in the dark and at the light intensity of 300 lux.

doi: 10.6342/NTU20230077

`

Chapter 4
Conclusion and Future Work

4-1 Conclusion

4-2 Future Work

4-2-1 Experimental Limits

4-2-2 Effect of Device Size

4-2-3 Effect of Gap Oxide Thickness

doi: 10.6342/NTU20230077

`

4-1 Conclusion

The thesis investigated the coupling effect between neighboring electrodes in concentric MIS(p) TDs and explored the potential of utilizing concentric MIS(p) TDs with CP-OX and MIS(p) TDs with ER-OX for photo sensing applications.

In Chapter 2, the coupling effect of the two categories of concentric MIS(p) TD was analyzed through the short-circuit current characteristics that should be close to zero in the dark. When the short-circuit current is not close to zero, it means that the device is affected by external factors. Our investigation found that applying a positive bias to the inner gate leads to a wide lateral fringe field distribution of the inner gate in the CP-OX case. As a result, the inner gate current flows towards the outer ring, resulting in a negative short-circuit current in the neighboring outer ring. However, in the ER-OX case, the outer ring is not affected by the neighboring inner gate due to its narrow lateral fringe field distribution, which keeps the short-circuit current of the sensing electrodes close to zero.

As we learned in Chapter 1, short-circuit current measurement can maintain photo sensing linearity, and adding a neighboring gate can enhance photosensitivity. Therefore, Chapter 3 focused on the applications and phenomena of two categories of concentric MIS(p) TD short-circuit operations in photo sensing. Applying a positive bias to the inner gate and short-circuiting the outer ring with the substrate enables the concentric MIS(p)TD with CP-OX to exhibit good linearity for photodetection. Moreover, due to the

doi: 10.6342/NTU20230077

`

coupling effect, it is possible to detect varying degrees of light intensity switching from negative to positive by adjusting the inner gate bias voltage.

In contrast, the concentric MIS(p) TD with ER-OX does not have a coupling mechanism when a positive inner gate bias is applied, resulting in similar performance as a single device during short-circuit operation. However, we still found a unique phenomenon. MIS(p) TD with ER-OX has no current flowing to the substrate due to the bias voltage of the outer ring being zero in the dark. As a result, the inner gate dominates the substrate current under this condition. When the light is illuminated, the photovoltaic effect generated additional photocurrent flows to the substrate from both the outer ring and inner gate. Consequently, the substrate current became the sum of the currents flowing through the two electrodes. In this way, we have obtained a better light-to-dark current ratio than a single device measured under positive bias.

In addition to the measurement of short-circuit current, an interesting measurement method was also proposed. We float the substrate, ground the inner center, and bias the outer ring. The concentric MIS(p) TDs can perform photo sensing in both negative and positive biases.

Through the analysis of the above applications and phenomena, it is believed that the results presented in this thesis and the proposed mechanism are crucial to the development of photo sensing.

doi: 10.6342/NTU20230077

`

4-2 Future Work

4-2-1 Experimental Limits

The experiment's LED light source had limited intensity, which prevented the study of situations greater than 500 lux. Future work will focus on studying the saturation limit of our photodetector.

4-2-2 Effect of Device Size

When the concentric device is illuminated, most of the charges are captured by the outer edge of the outer ring (sensor) through the fringe field [22]. This means that the larger the outer perimeter of the outer ring, the stronger the photovoltaic effect, and the greater the additional photocurrent generated. Since the outer perimeter of the outer ring dominates the photovoltaic effect, adjusting the size of the inner center does not impact the photovoltaic effect of the outer ring. However, reducing the size of the inner circle weakens the coupling effect of concentric MIS(p) TDs with CP-OX. As explained in Section 3-2-2, a weaker gate coupling effect implies that the gate has a reduced impact on sensor linearity distortion, resulting in the sensor current changing more similarly to that of a single device. Consequently, the performance may exhibit improved linearity in weak light. In addition, the separation between the two electrodes is also a crucial factor that affects the coupling effect [13]. As the gap distance between the two electrodes increases, the coupling effect weakens. Therefore, to widen the linearity range and maintain the

doi: 10.6342/NTU20230077

`

characteristics of positive and negative switching that identify light intensity due to the coupling effect, it may be worthwhile in future studies to experiment with increasing the gap distance between the two electrodes and reducing the size of the inner gate in concentric MIS(p) TDs with CP-OX.

4-2-3 Effect of Gap Oxide Thickness

We investigate the effect of the oxide layer thickness between two neighboring electrodes on the MIS(p) TD, which has not been studied in the past. Fig. 4-1 shows the *I-V* curves of single center devices, single ring devices, and concentric devices with varying gap oxide thicknesses ($d_{\mathrm{ox(g)}}$). Figs. 4-1(a) and (c) correspond to MIS(p) TDs with ER-OX and MIS(p) TDs with CP-OX, respectively, as described in previous chapters. Fig. 4-1(b) shows the results after etching the SiO_2 in the gap followed by 3 minutes of anodization, resulting in a thinner SiO_2 layer growing in the gap. Fig. 4-1(d) shows the results after etching the Al in the gap followed by 3 minutes of anodization, leading to a thicker SiO_2 layer growing in the gap. The insets in the four figures are schematic diagrams of their structures. The results show that Figs. 4-1(a) and (b) exhibit similar behavior. The current curve of the inner center of the concentric device in the positive bias region is similar to that of the single center device, indicating no coupling effect. In contrast, for Fig. 4-1(c), the current curve of the inner center of the concentric device in the positive bias region is similar to that of the single ring device, implying a coupling effect between

doi: 10.6342/NTU20230077

`

the inner center and the outer ring. Notably, the inner center current curve of the concentric device in the positive bias region in Fig. 4-1(d) falls between that of the single center and the single ring device. This observation suggests that the thickness of the raised gap oxide could alter the lateral fringe field distribution and weaken the coupling effect between the two electrodes. The reason behind these results requires further investigation in the future. Furthermore, the potential impact and application of this structure, which weakens the coupling effect, in light sensing or other aspects can be further analyzed in detail.

doi: 10.6342/NTU20230077

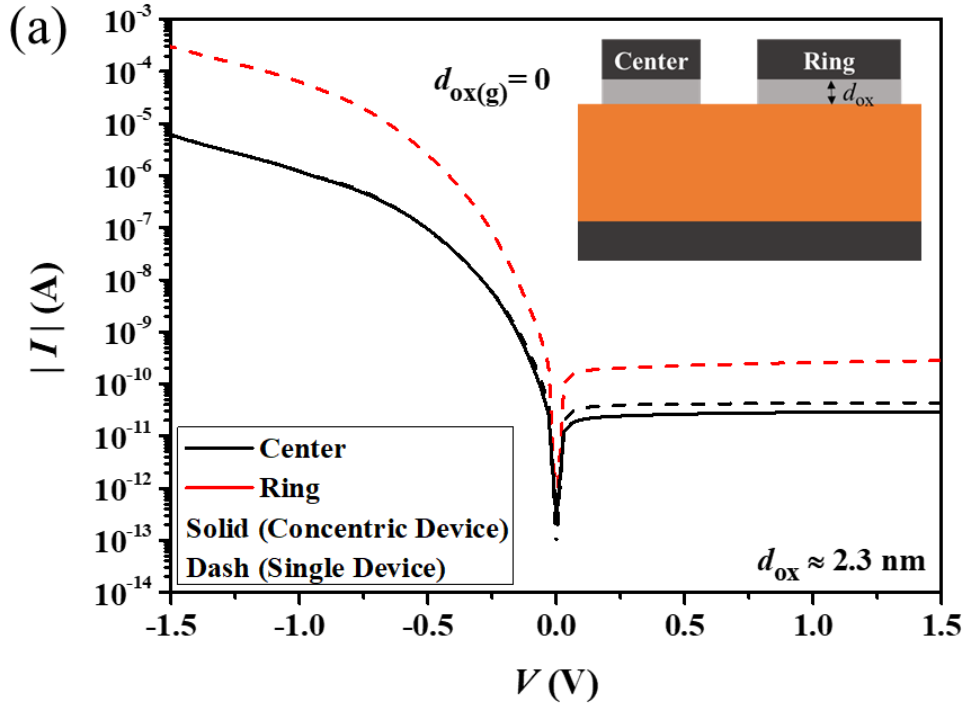

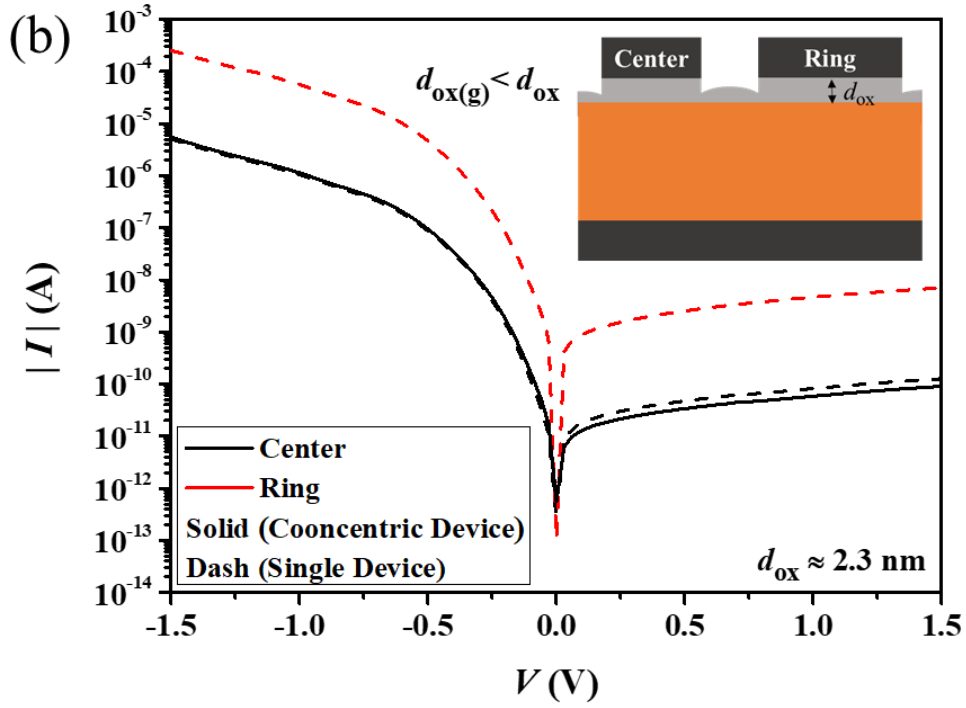

(to be continued)

doi: 10.6342/NTU20230077

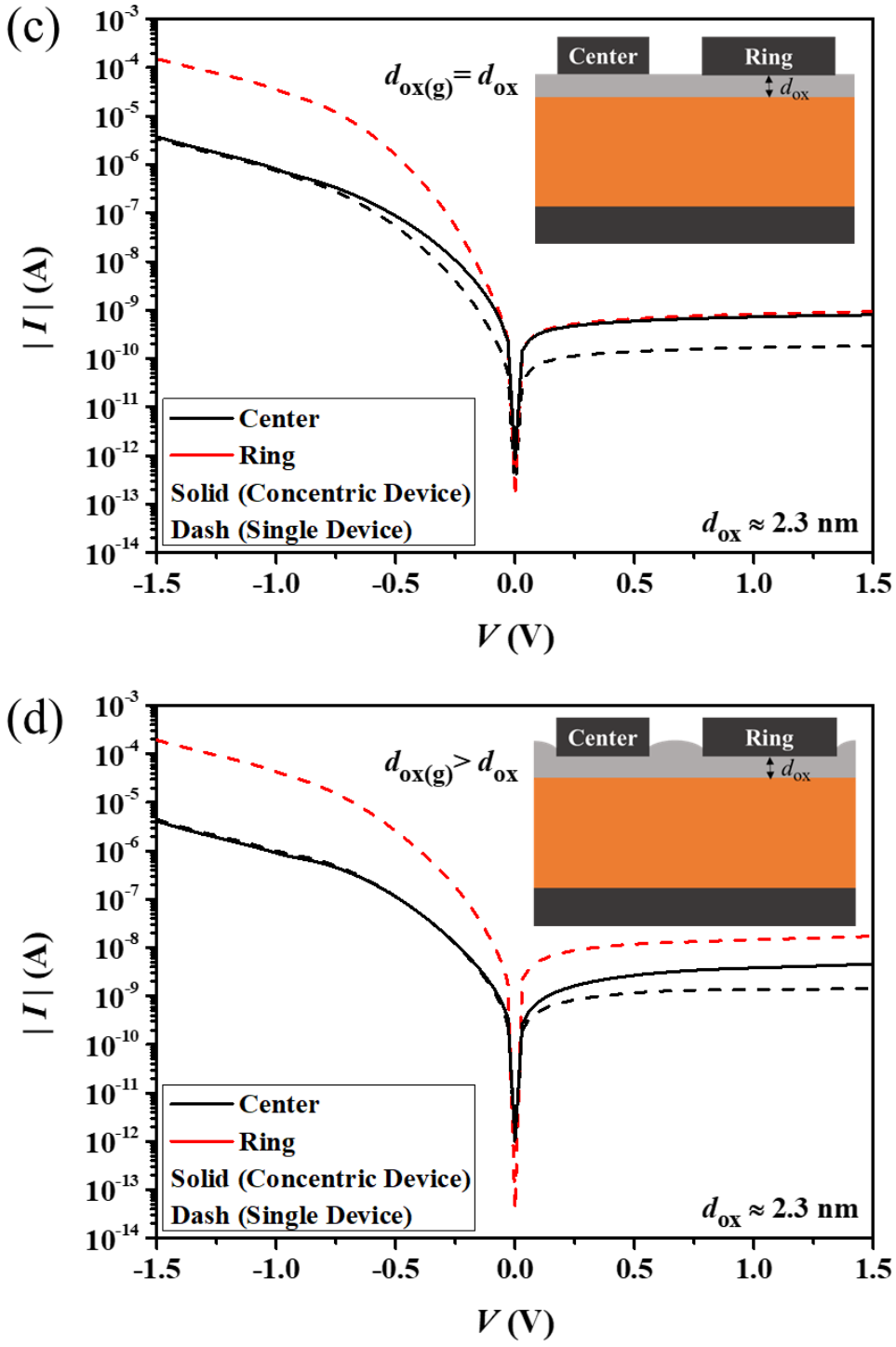

Fig. 4-1. *I-V* curves of concentric center, single center, single ring MIS(p) TDs with different gap oxide thickness. The four graphs are (a) edge-removed oxide (ER-OX), (b) thinner gap oxide, (c) co-planar oxide (CP-OX), and (d) thicker gap oxide. The insets are schematic diagrams of the structure.

doi: 10.6342/NTU20230077

`

References

[1] Y. -H. Tai, C. -C. Tu and S. Yeh, “Using Amorphous Silicon Gap-Type Thin Film Transistor as Ambient Light Sensors and Proximity Sensors for Smartphones,” IEEE Sensors Lett., vol. 3, no. 10, pp. 1-4, Oct. 2019, Art no. 1500304, doi: 10.1109/LSENS.2019.2940763.

[2] D. Joos, “Integrated EMI Detector as Essential Safety Mechanism in Automotive Sensor Applications,” ISEMC, 2022, pp. 451-456, doi: 10.1109/EM-CEurope51680.2022.9901193.

[3] F. -H. Chen et al., “Compact Optical Sensor Based on Thin-Film Transistors for Large Interactive Displays Using Red/Green/Blue Laser Pointers,” IEEE Electron Device Lett., vol. 41, no. 6, pp. 876-879, June 2020, doi: 10.1109/LED.2020.2987031.

[4] A. Radoi, M. Dragoman and D. Dragoman, “Plasmonic ambient light sensing with MoS2-graphene heterostructures,” Phys. E, vol. 85, pp. 164-168, Jan. 2017, doi: 10.1016/j.physe.2016.08.026.

[5] X. Mo et al., “Highly-efficient all-inorganic lead-free 1D CsCu2I3 single crystal for white-light emitting diodes and UV photodetection,” Nano Energy, vol. 81, pp. 105570, Mar. 2021, doi: 10.1016/j.nanoen.2020.105570.

[6] W. Huang et al., “Facile fabrication and characterization of two-dimensional bismuth

doi: 10.6342/NTU20230077

(III) sulfide nanosheets for high-performance photodetector applications under ambient conditions," Nanoscale, vol. 10, no. 5, pp. 2404-2412, Dec. 2017, doi: 10.1039/C7NR09046C.

[7] Y. -K. Lin and J. -G. Hwu, "Photosensing by Edge Schottky Barrier Height Modulation Induced by Lateral Diffusion Current in MOS(p) Photodiode," IEEE Trans. Electron Devices, vol. 61, no. 9, pp. 3217- 3222, Sept. 2014, doi: 10.1109/TED.2014.2334704.

[8] C.-H. Lin and C. W. Liu, "Metal-insulator-semiconductor photodetectors," Sensors, vol. 10, no. 10, pp. 8797–8826, Sep. 2010, doi: 10.3390/s101008797.

[9] C.-F. Yang and J.-G. Hwu, "Role of fringing field on the electrical characteristics of metal-oxide-semiconductor capacitors with co-planar and edge-removed oxides," AIP Adv., vol. 6, no. 12, Dec. 2016, doi: 10.1063/1.4971845.

[10] J. Wilson, J. F. Hawkes, Optoelectronics an introduction, 3rd ed., Prentice Hall, pp. 324-329, 1998.

[11] C. -S. Liao and J. -G. Hwu, "Subthreshold Swing Reduction by Double Exponential Control Mechanism in an MOS Gated-MIS Tunnel Transistor," IEEE Trans. Electron Devices, vol. 62, no. 6, pp. 2061-2065, June 2015, doi: 10.1109/TED.2015.2424245.

[12] J. -Y. Lin, "Effects of Neighboring Oxide Charge on The Characteristics of Metal-

doi: 10.6342/NTU20230077

Insulator-Semiconductor Tunnel Diode," M. S. thesis, Dept. Elect. Eng. Nat. Taiwan Univ. Taipei, Taiwan, R.O.C., 2022, doi: 10.6342/NTU202201070.

[13] W. -T. Hou and J.-G. Hwu, "Photo response enhancement in MIS(p) tunnel diode via coupling effect by controlling neighboring device inversion level," ECS J. Solid State Sci. Technol., vol. 6, no. 10, pp. Q143–Q147, Nov. 2017, doi: 10.1149/2.0031712jss.

[14] Y. -H. Chen and J. -G. Hwu, "Light Sensing Enhancement and Energy Saving Improvement in Concentric Double-MIS(p) Tunnel Diode Structure With Inner Gate Outer Sensor Operation," IEEE Trans. Electron Devices, vol. 65, no. 11, pp. 4910-4915, Nov. 2018, doi: 10.1109/TED.2018.2871071.

[15] C. -Y. Huang and J. -G. Hwu, "Enhanced Photo Sensing and Lowered Power Consumption in Concentric MIS Devices by Monitoring Outer Ring Open-Circuit Voltage With Biased Inner Gate," IEEE Trans. Electron Devices, vol. 68, no. 7, pp. 3417-3423, July 2021, doi: 10.1109/TED.2021.3082813.

[16] M. -H. Yang and J. -G. Hwu, "Influence of neighboring coupling on metal-insulator-semiconductor (MIS) deep-depletion tunneling current via Schottky barrier height modulation mechanism", J. Appl. Phys., vol. 121, no. 15, pp. 154504-1–154504-6, Apr. 2017, doi: 10.1063/1.4981891.

[17] S. M. Sze and K. K. Ng, Physics of Semiconductor Devices, New York, NY,

doi: 10.6342/NTU20230077

USA:Wiley, pp. 671-674, 2007.

[18] Z. Bielecki et al., “Review of photodetectors characterization methods,” in Bull. Pol. Acad. Sci. Tech. Sci., 2022, vol. 70, no. 2, doi: 10.24425/bpasts.2022.140534

[19] C.-H. Oh, J.-I. Shim, and D.-S. Shin, “Current–voltage characteristics of InGaN/GaN blue light-emitting diodes investigated by photovoltaic parameters,” Jpn. J. Appl. Phys., vol. 58, no. 1, Nov. 2018, doi: 10.7567/1347-4065/aae92f.

[20] M. A. Green, F. D. King and J. Shewchun, “Minority carrier MIS tunnel diodes and their application to electron-and photo-voltaic energy conversion—I. Theory,” Jpn. J. Appl. Phys., vol. 17, no. 6, pp. 551-561, June 1974, doi: 10.1016/0038-1101(74)90172-5.

[21] M. A. Green, F. D. King and J. Shewchun, “Minority carrier MIS tunnel diodes and their application to electron-and photo-voltaic energy conversion—II. Experiment,” Jpn. J. Appl. Phys., vol. 17, no. 6, pp. 563-572, June 1974, doi: 10.1016/0038-1101(74)90173-7.

[22] Yu-Hsuan Chen and Jenn-Gwo Hwu, “Roles of Inner and Outer Fringe and Asymmetric Coupling Effect in Concentric Double-MIS(p) Tunneling Diodes,” Electrochemical Society Transactions, Vol.89, No.3, 121~131, Jun. 2019, doi: 10.1149/MA2019-01/23/1199.

doi: 10.6342/NTU20230077